TISSUE ENGINEERING
Volume 13, Number 4, 2007

DOI: 10.1089/ten.2006.0321

Small-Diameter Porous Poly (ε-Caprolactone) Films Enhance Adhesion and Growth of Human Cultured Epidermal Keratinocyte and Dermal Fibroblast Cells

JAMES R. MCMILLAN, M.Sc., Ph.D.,[1,2] MASASHI AKIYAMA, M.D., Ph.D.,[1] MASARU TANAKA, Ph.D.,[2] SADAKI YAMAMOTO, Ph.D.,[2] MAKI GOTO, Ph.D.,[1] RIICHIRO ABE, M.D., Ph.D.,[1] DAISUKE SAWAMURA, M.D., Ph.D.,[1] MASATSUGU SHIMOMURA, Ph.D.,[2] and HIROSHI SHIMIZU, M.D., Ph.D.[1]

ABSTRACT

Autologous keratinocyte grafts provide clinical benefit by rapidly covering wounded areas, but they are fragile. We therefore developed biocompatible hexagonal-packed porous films with uniform, circular pore sizes to support human keratinocytes and fibroblasts. Cells were cultured on these porous poly (ε-calprolactone) films with pore sizes ranging from novel ultra-small 3 μm to 20 μm. These were compared with flat (pore-less) films. Cell growth rates, adhesion, migration, and ultrastructural morphology were examined. Human keratinocytes and fibroblasts attached to all films. Furthermore, small-pore (3-5 μm) films showed the highest levels of cell adhesion and survival and prevented migration into the pores and opposing film surface. Keratinocyte migration over small-pore film surface was inhibited. Keratinocytes optimally attached to 3-μm-pore films due to a combination of greater pore numbers (porosity), a greater circumference of the pore edge per unit surface area, and greater frequency of flat surface areas for attachment, allowing better cell–substrate and cell–cell attachment and growth. The 3-μm pore size allowed cell–cell communication, together with diffusion of soluble nutrients and factors from the culture medium or wound substrate. These characteristics are considered important in developing grafts for use in the treatment of human skin wounds.

INTRODUCTION

THERE HAVE BEEN NUMEROUS REPORTS OF micro-scale and nano-scale structured materials with biologically significant properties using basic chemical composition and micro- or nano-scale structural features that may influence cell characteristics grown on these materials.[1–5] Studies examining this phenomenon include those exploring fibrovascular connective tissue cultured on foams,[6,7] osteoblasts grown on porous surfaces,[8,9] tissue fibroblasts on porous membranes,[10] and mouse 3T3 fibroblast-maintained porous collagen–glycosaminoglycan scaffolds.[11] The typical cell responses to nano- and micro-scale structure and geometry include changes in cell adhesion, proliferation, and survival on smaller-scale structures and altered morphology, including cell size, shape, and orientation.[6,7,12,13] Material pore size has emerged as a significant factor affecting cell adhesion and growth on culture substrates; however, the pore shape in many experimental biomaterials has been irregular and had poor uniformity of pore distribution, with variable, generally poorly controlled pore size.[7,10,14,15] We have developed a low-cost process of porous film manufacturing using biocompatible poly (ε-caprolactone) (PCL) material that produces a regular, controlled pore size and a regular, hexagonally packed pore distribution on a flat film.[16–19]

[1]Department of Dermatology, Hokkaido University, Graduate School of Medicine, Sapporo, Japan.
[2]Creative Research Initiative Sousei, Faculty of Science, Hokkaido University, Sapporo, Japan.

Unsupported human skin grafts in current use are composed of keratinocyte sheets and are thin, fragile grafts that must be removed from a donor site, causing further patient injury, and later applied to pre-prepared, cleaned wounded areas to aid rapid wound coverage and achieve effective results. Additional support of these cultured autologous grafts, especially during the handling process, is desirable to improve graft application. Aliphatic polymers such as those made from PCL provide sufficient strength, support, and flexibility and are also biocompatible and biodegradable in the human body. (They are already being used in surgical sutures and blood vessel stents or supports.[13,20]) The porous film also provides an occlusive surface to separate distinct groups of cells on opposite sides; the size of the film pores can precisely control the wound bed connective tissue cells and cultured epithelial cells and the extent to which these two cells types interact.[21] In addition, the center of the pore can itself be used to store or protect biological structures, for example, adhesion components or growth factors encapsulated in controlled-release technologies. Previously, the range of pore sizes that have been regularly and uniformly fabricated has been between 5 and 20 μm in diameter because of limitations in the polymer and solvent used.[19,22,23] Here, we demonstrate that this limit has been extended to grow skin-derived cells on the smallest pores (3 μm) that can be fabricated using self-organizing processes. The precise control of regular pore size limits cell adhesion and communication as well as allowing storage of bioactive compounds provides an important benefit to using the porous films as graft substrates.

We have developed a way to easily and cheaply prepare a regular, patterned surface on which cells can be grown that allow it to be used as a graft to improve wound healing. Our novel porous PCL films (devised and patented by Creative Research Initiative Sousei, Hokkaido University, see patents by Tanaka et al.[1] McMillan et al.[2]) have been tested as a biodegradable platform to support cultures of various human cells.[16,18,24,25] Furthermore, we report here the first fabrication and use of ultra-small-pore-size films with 3-μm-sized pores and report the effects culturing the 2 main skin-derived cells, keratinocytes and fibroblasts, grown on this substrate.

To investigate the effect regular porous films have on monocultures of skin cells, we have investigated the properties of cultured human epidermal keratinocyte and dermal fibroblast cell adhesion, migration, growth, and morphology on different-sized pore substrates. The aim of this study is to enhance our understanding of the processes of cell–substrate interactions and how these factors affect cell adhesion, growth, migration, and morphology. This knowledge will allow us to make further improvements to optimize skin graft efficacy and improve wound healing.

[1]Biodegradable honeycomb films for tissue engineering scaffolds (Patent number: 1999-340568(JP). Application date: 1999/11/30.) Biomedical devices (Patent number: 2001-342484 (JP). Application date: 2001/11/07.)

[2]Porous honeycomb films: applications for cultured human keratinocyte and fibroblast composite grafts and human skin equivalents (Patent number: 2005-188948(JP). Application date: 2005/06/28.)

MATERIALS AND METHODS

Preparation of porous films

The porous PCL uniform 3-dimensional porous films were manufactured using previously described procedures.[16,26,27] Films were disinfected and sterilized (using ethanol and ultraviolet light sterilization), washed, an dair dried, and trapped air was removed using a combination of serial ethanol and sterile 0.1 M Dulbecco's phosphate buffered saline (PBS) washes (Invitrogen/Gibco, BRL, Carlsbad, CA). The sterilized porous films were then directly seeded with monocultures of keratinocytes or fibroblasts. The production procedure uses polymer–solvent mixtures to form perfectly spherical solvent-filled spaces, and thereby pores, in the films. Thus, pore size and depth are intrinsically linked.

Cell sources

The cells (keratinocytes and fibroblasts) were seeded on the upper surface of the film only. Fibroblast cells were sustained in Dulbecco's modified Eagle medium (DMEM) with 10% fetal calf serum, penicillin, and streptomycin (Cambrex, Walkersville, MD) for 24 h to 10 days. Keratinocytes were cultured in keratinocyte growth medium (KGM) I (Cambrex, Walkersville, MD) for between 24 h and 10 days. Normal human neonatal foreskin keratinocytes (Cambrex) were grown in KGM I culture medium (Clonetics, Walkersville, MD) until passage 2 or 3 (P2/P3). The cells were then trypsinized and stored in 10% dimethyl sulfoxide (DMSO) under liquid nitrogen until needed. Normal human dermal fibroblasts were obtained (Cambrex) and grown in DMEM (Cambrex) until P2. Cells were then trypsinized and stored in 10% DMSO under liquid nitrogen until required.

Cell adhesion and growth assays

Normal human neonatal keratinocytes (P2/P3) or dermal fibroblasts (P2) were grown in appropriate culture medium. Cells were trypsinized and counted and 3×10^5 cells plated onto 16-mm-diameter sterilized circular glass-supported substrates including flat (pore-less) PCL film and porous PCL films. This density has previously been determined to be more than sufficient for proper seeding of keratinocyte grafts.[28] Cells were left to adhere for 2 or 24 h to these films with various sized pores. After this time period, the plates were washed 4 times in sterile 0.1 M Dulbecco's PBS and the numbers of live keratinocytes counted after a 5-min incubation with 0.05 μg/mL of acetoxymethyl ester (AME,

C-369), a fluorescent marker for live cells (Molecular Probes, Eugene, OR), in PBS followed by two 5-min washes each in PBS and then DMEM. Only live cells (keratinocytes or fibroblasts) are able to deacetylate the non-fluorescent protein, converting it into fluorescent form. Attached cells were immediately counted using an Olympus Fluoview FV300 confocal and IX70 inverted microscope (Olympus, Tokyo, Japan). Only attached, live, uniformly fluorescent cells were counted on each substrate at a single time point (24 h after initial plating). The mean number of live cells per high power field ($n > 10$) per substrate was calculated. This experiment was repeated 3 times. The treatment groups were compared using one-way analysis of variance (ANOVA) and two sample t-tests using the Minitab statistical package (Minitab Inc., University of Pennsylvania, Philadelphia, PA) at $p < 0.05$ or <0.01 showing significant effects.

For the cell-growth assay, P2-P3 cells were grown on flat or porous films, as previously described,[24] and grown in appropriate culture medium. At specific time points (24, 48, and $\geq$144 h) the plates were washed 4 times in sterile 0.1 M Dulbecco's PBS and the numbers of live cells counted as previously described one directly from phase-contrast photomicrographs. Attached cells were counted using an Olympus IX70 inverted Fluoview FV300 confocal microscope. The numbers of live cells per high-power field ($n > 10$) were calculated per substrate group. Statistical analysis was performed between the treatment groups using one-way ANOVA and two sample t-tests using the Minitab statistical package. The results are shown in Figure 1B and D. This experiment was repeated 3 times.

Migration assay

Normal control P3 keratinocytes or fibroblasts were plated onto substrates (flat calprolactone or porous films). Cells were grown on various substrates in KGM I (keratinocytes) or DMEM (fibroblasts, Clonetics). Cells were grown at between 1×10^5 and 3×10^5 cells per 16-mm well on various substrates as previously described and placed in a temperature- and carbon dioxide (CO_2)-controlled microscopic stage while

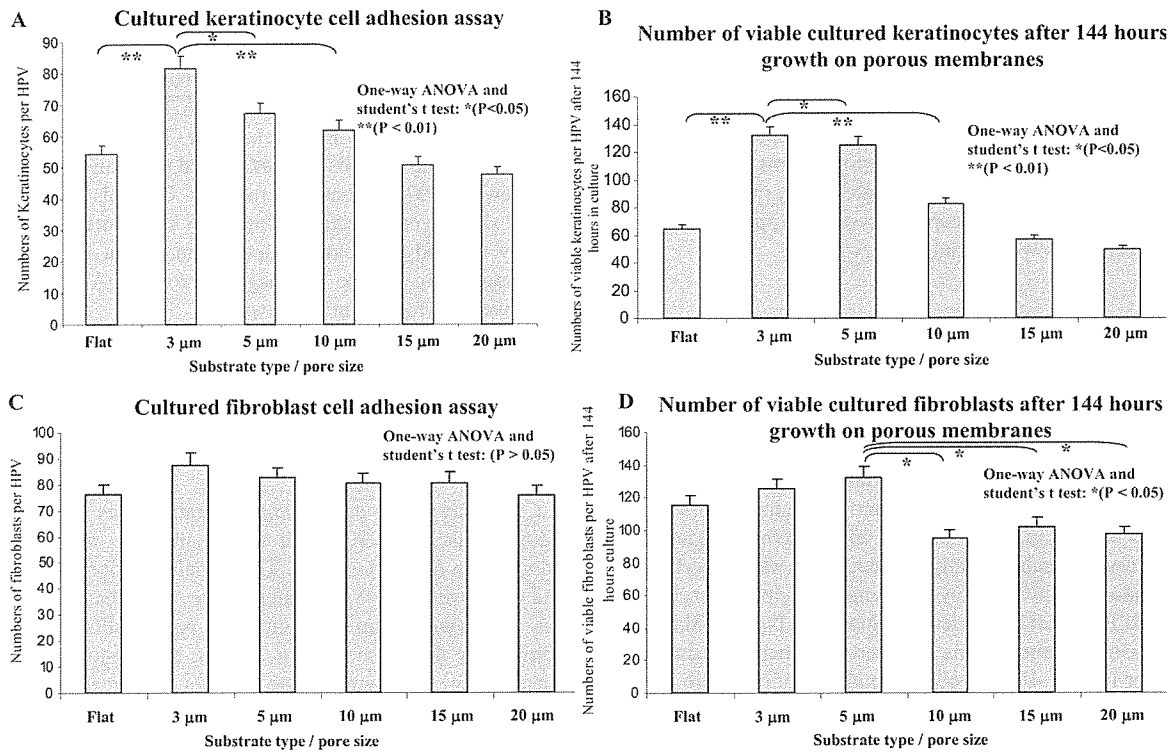

FIG. 1. Keratinocytes show greater increases in cell-substrate adhesion and growth than fibroblasts on porous poly(ε-caprolactone) films. Keratinocyte adhesion assays over 24 h (**A**) demonstrated statistically significantly ($p < 0.01$) greater keratinocyte adhesion between 3 μm porous films than between all other larger films. (**B**) Keratinocyte growth assay over 144 h (6 days) showed a similar ranking but also more-significant differences between 3-μm and other films. Fibroblast adhesion rates over 24 h showed no significant changes when these cells were plated on different films (**C**). (**D**) The fibroblast growth rate over 144 h showed moderate differences ($p < 0.05$) between the flat, 3-μm, and 5-μm group and the larger-pore 10-μm, 15-μm, and 20-μm group. For fibroblasts, the 5-μm films appeared optimal for growth. Statistical analysis: one-way analysis of variance (ANOVA) and Student t tests. *ANOVA, $p < 0.05$, **$p < 0.01$). Error bars 1 = standard deviation.

cells were observed using video microscopy using an INU-NI series microscope stage fitted to an inverted TE 2000 microscope (Nikon, Tokyo, Japan). Single-cell migration assays using time-lapse digital video microscopy were performed for periods of between 8 and 24 h. The number of cells observed using video microscopy was greater than 50 cells per group. Cells were observed using a time-lapse video interval of 5 min, and the distance traveled was observed using a precalibrated scale and MCID/M2 image analysis software (Imaging Research Inc., Ontario, Canada). Cell viability counts were confirmed after 5 min incubation with 0.05 μg/mL of C-369 AME, a fluorescent marker for live cells (Molecular Probes), and examination under a confocal microscope as previously described. The average distance traveled per hour was calculated for each cell type on each substrate. Statistical analysis was performed to compare the treatment groups using one-way ANOVA and two sample t-tests using the Minitab statistical package.

Scanning electron microscopy

Cells grown on various substrates for 48 h were fixed in 2% glutaraldehyde for at least 4 h and processed for routine scanning electron microscopy (SEM). Briefly, samples were dehydrated in a graded ethanol series, treated twice with isoamyl acetate, and critical point CO_2 dried using a Hitachi HCP-2 followed by platinum-palladium sputter coating in a Hitachi E-1030 (Tokyo, Japan). Specimens were examined using a Hitachi S-4500 scanning electron microscope fitted with a digital image capture system. Approximately 200 adherent cells were examined per group.

Transmission electron microscopy

Cells grown on films for 48 h were fixed in 2% glutaraldehyde solution, post-fixed in 1% osmium oxide, dehydrated, and processed for conventional electron microscopic observation according to the methods described previously.[29] Alternatively, samples were dehydrated using a graded ethanol series but were not treated with propylene oxide. Instead they were washed in 100% ethanol and a methanol–acetic acid mixture and subsequently embedded in white acrylic resin (London Resin Company, Reading, UK) or Lowicryl K11M (Ladd Research Industries, Burlington, VT) to avoid harmful film–solvent interactions that were polymerized using ultraviolet light at 4°C for 48 h. Semithin sections were cut and stained with Richardson's stain.[30] Samples were cut, stained with uranyl acetate and lead citrate, and viewed under a Hitachi H-7100 transmission electron microscope at 75 kV.

Confocal immunofluorescence microscopy

Indirect immunofluorescence was performed as previously described[29] using 3-μm porous films with keratinocyte and 5-μm porous films and fibroblast monocultures in addition to cryostat normal skin sections. The mouse monoclonals M3F7 and LH7:2, recognizing collagen IV and collagen VII, respectively, were used at neat and 1 in 2 dilutions.[29] M3F7 were obtained from the Developmental Studies Hybridoma bank, University of Iowa. A laminin 5 antibody, GB3, directed against the laminin 5 α2 chain (Harlan Sera Laboratory, Loughborough, UK), mouse immunoglobulin (Ig)G vinculin VIN-11-05 (Sigma, St Louis, MI) 1 in 100 dilution, desmoplakin (11F5) used at 1 in 50 dilution, and E cadherin HECD1 were used. 4C7 monoclonal antibody recognizing the laminin 10 was used diluted 1 in 25.[29] The following primary antibodies and sera were also used in this study: anti-human keratin 14, clone LL001 diluted 1 in 2 (gifts from B. Lane, Dundee, UK), anti-talin, TD77 mouse antibody diluted 1 in 200, mouse anti-collagen I (1 in 100), and rabbit polyclonal vimentin diluted 1 in 200 (Abcam, Cambridge, UK) against synthetic talin (amino acids 2269-2541) encoding the polypeptide f actin binding region. Staining for actin was performed using phalloidin and rabbit anti-human actin rabbit IgG antisera (Biomedical Technologies, Stoughton, MS).

Cell and film cryostat sections were fixed in acetone methanol and incubated with primary antibodies and antisera. Sections were incubated with secondary antibodies conjugated to fluorescein isothiocyanate (FITC; rabbit anti-mouse IgG or goat anti-rabbit IgG; 1:200; Dako, Tokyo, Japan). Sections were then labeled with a Topro 3 nuclear counterstain (Jackson Immuno-Research, West Grove, PA, diluted 1 in 20,000). The sections were examined using an Olympus Fluoview FV300 confocal microscope. Controls included normal skin cryostat sections, with PBS substituted for the primary antibody, myeloma supernatant, or an irrelevant immunoglobulin isotype as a negative control. All experiments were performed at least twice.

RESULTS

Cell adhesion and growth assays

Cell adhesion on porous films. Keratinocytes (Fig. 1A) and fibroblasts (Fig. 1C) were able to attach to, adhere to, and grow on all porous films. The initial adhesion of keratinocytes (over 24 h) was greater on the small-diameter porous films (with 3 μm producing the best results, closely followed by the 5-μm, 10-μm, 15-μm, and 20-μm porous films, see Fig. 1A). Keratinocyte adhesion was greatest using the smaller-diameter porous film pores (with 3 μm producing the best results, followed closely by the 5-μm film, Fig. 1). However, overall, cell adhesion to the porous films was significantly greater in human dermal–derived fibroblasts than in human epidermal keratinocytes (Fig. 1A vs 1C). Fibroblasts, overall, showed far less-significant differences (Fig. 1C, $p > 0.05$) between adhesion rates on different films, with only a slight increase in adhesion 3 μm compared to sequential minimal decreases in 5 μm, 10 μm and flat surfaces. These data are in broad agreement with our previous

report that demonstrated high levels of adhesion to various porous films shown by the mouse NIH 3T3 fibroblast cell line.[24]

Cell growth rates. Cell growth rates were assessed for up to 6 days. All culture samples were seeded with the same number of cells on each substrate in each well. After 6 days of culture, live cells were stained and cells counted per randomly selected high-power field. Keratinocytes showed the highest proliferation and/or survival rates on 3-μm porous films, although the 5-μm porous films also demonstrated a slightly slower growth rate. These two samples' growth rates were significantly higher than those of any of the larger-pore films (10 μm > 15 μm > 20 μm) or flat substrate.

Fibroblasts showed similar, high growth levels on the 5-μm and 3-μm pore films and flat substrates. However, they also showed significantly lower growth rates on the larger-pore films (10-μm, 15-μm, and 20-μm pores) than on those with smaller pores. This was an approximately 25% to 30% lower growth rates on films with 10-μm pores than on those with 5-μm pores.

Cell migration over the film surface

Lateral cell migration over the surface of the porous film was analyzed using time-lapse video and image analysis and showed that keratinocyte migration rates were lower after plating of cells onto any PCL film than for keratinocytes grown on plastic[31] (Fig. 2, grey bar flat (poreless) PCL vs porous PCL films). Fibroblast migration was significantly less ($p < 0.05$ and $p < 0.01$) but not completely inhibited after plating on porous films, causing reductions of up to 30% (Fig. 2 white bars flat PCL vs 3-μm and 5-μm PCL film, respectively). The differences here reflect severely slower keratinocyte migration rates on any PCL film than the reported migration of keratinocytes on plastic[31] and gradually slower migration rates of fibroblasts grown on 3-μm and 5-μm films (respectively) than for those grown on pore-less flat films.

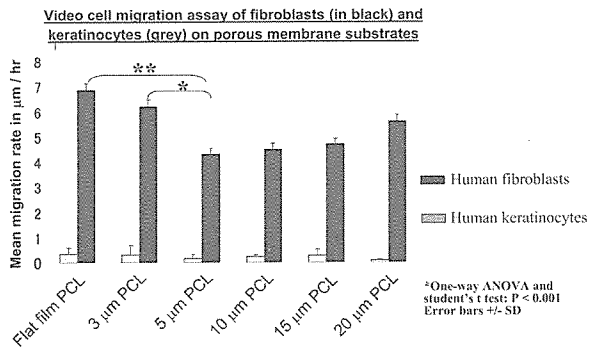

FIG. 2. Video microscopy–assessed migration showed higher migration rates for fibroblasts than for keratinocytes when maintained on porous films. Keratinocyte migration was inhibited on porous membranes, whereas fibroblasts showed the highest migration rates on flat pore-less films, only moderate reductions in migration on 3-μm films and more significant reductions on 5- to 10-μm films. Surprisingly fibroblast migration showed a modest increase on the 20–μm films. Statistical analysis: one-way analysis of variance and Student t tests. $*p < 0.05$, $**p < 0.01$). Error bars 1 = SD.

Migrating cells can cross films with smaller pore sizes more easily than they can cross films with large pores. In addition, the length of pore edge per specific unit surface area is greatest in the small-pore film, which enables cells to use plasma membrane lamleopodia extensions (presumably containing focal contacts) to gain better adhesion on the underlying surface and allow better signal transduction that enable still better adhesion and growth.

Scanning electron microscopy

Keratinocytes seeded onto flat pore-less surfaces attached quickly, spread, and flattened within 2 to 4 h of plating (and were examined using phase contrast microscopy). Cells attached to the underlying substrate using thin filopodial extensions of the plasma membrane that resembled focal adhesions (Fig. 3A–D, white arrows). Keratinocytes subsequently formed small colonies of cells that grew and migrated over the flat films. Keratinocytes on all sizes of porous substrates (Fig. 3B–D) took longer than 48 h to spread (Fig. 3B). Keratinocytes seeded near adjacent cells or those that produced daughter cells after mitotic division maintained desmosome connections (white arrowheads in Fig. 3C) between adjacent cells. Cells were typically positioned over adjacent pores (see Fig. 3B, C). Ultimately, keratinocytes plated on films with pores of any size spread and flattened, covering the film surface with a diameter of as much as 30 to 40 μm (Fig. 3D). Eventually, keratinocytes characteristically formed thin, flat, "fried egg" shapes that covered the pores and surface of the film in equal proportion (Fig. 3D). On the largest-pore films (15–20 μm) occasional individual keratinocytes could be seen within the pores of the film (data not shown).

Fibroblasts grown on flat films quickly attached, spread, and flattened within 3 h (Fig. 3E). Fibroblasts on porous films spread more slowly than on flat films and initially maintained an elongated shape but without significant flattening (Fig. 3F vs E). Eventually, fibroblasts spread and formed flattened shapes covering the porous films as the number of cells increased (Fig. 3G). In larger-pore films (≥5 μm), entire cells were observed that had entered pores, and the cell body passed into the pore space between the upper and lower layers of the film (Fig. 3H, inset). Fibroblasts, because of their thinner, more-elongated shape, were much more frequently observed entering the large film pores (Fig. 3H and inset) than keratinocytes.

Transmission electron microscopic analysis of cells grown on support films

Transmembrane cell migration keratinocytes. Semithin sections showed the basically normal morphology of keratinocytes and fibroblasts grown on flat and porous film supports

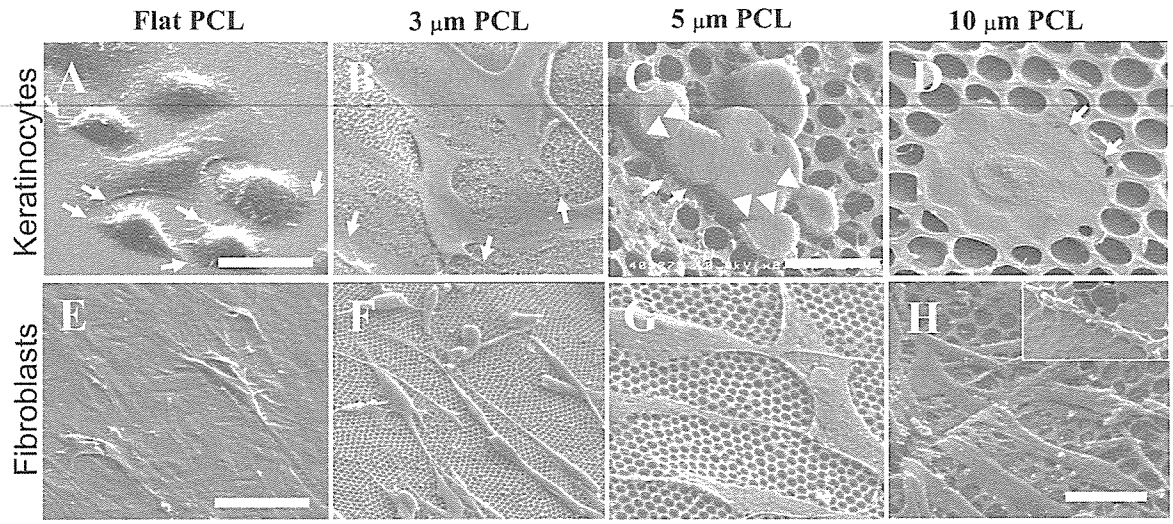

FIG. 3. Scanning electron micrographs showing the morphology of cells grown on flat and porous films after 48 h in culture. Keratinocytes (**A–D**) and fibroblasts (**E–H**) exhibit good cell–substrate attachment on all the surfaces by means of cell projections (filopodia) attaching to the surfaces (arrows in **A**). These cell projections resembled focal adhesion associated lamellipodia/filopodia (arrows in **A–D**). Keratinocytes were slower to spread than fibroblasts but formed flatter, more-rounded cells (**B–D**). Adjacent keratinocytes were able to form close cell–cell associations at possible sites of cell-junction formation (arrowheads in **C**). Conversely, fibroblasts formed small round cells but rapidly (in <1 h) elongated becoming spindle-like cells containing nuclear bulges eventually becoming 25 μm in length. On larger porous films with pores 10 μm and greater, cell processes and entire fibroblasts entered the pores (see inset in **H**). Scale bars (**A, C, E**) 15 μm, (**B, D, F, G, H**) 30 μm.

(Fig. 4A–J). The black dashed lines highlight the upper surface of the flat or porous film (Fig. 4A–J). Keratinocytes seeded on porous films initially showed a rounded morphology and typically sent down small cytoplasmic projections extending 1 to μm into the pores (arrows in Fig. 4C, E, G, I). The number of pores per unit surface area were highest in small-pore (3 μm, Fig. 4C) films and lowest on the large-pore films (15 μm, Fig. 4I; 20 μm, Fig. 4K). (For review of porous film properties, see[22].) This means that keratinocytes grown on small-pore film could form greater numbers of cell projections into the pores per unit surface area than in larger-pore films. In the large-pore films, entire necrotic keratinocytes with pyknotic nuclei were observed within the open pore spaces (Fig. 4K, arrows).

As previously demonstrated using SEM, fibroblasts grown on all porous films showed a flatter morphology than keratinocytes (Fig. 4B). Fibroblasts were also able to extend variable length cell processes and entire cells into the pores, but because these cells were generally longer and thinner than keratinocytes, entire cells were able to enter any pores larger than 5 μm (arrows in Fig. 3F, H, J, L). As the pore size increased beyond 5 μm, increasing numbers of fibroblasts were able to migrate and multiply in the center of the porous films (Fig. 3F, H, J, L).

Transmembrane cell migration. The transmembrane migration of keratinocytes was completely prevented using films with smaller-diameter pored (with the 3- and 5-μm films most effectively preventing transmigration). Only the smallest-pore (3 μm) films were effective at preventing the transmembrane transfer of migrating fibroblasts cells into the spaces in the center of the film. The ratio of pore-size diameter to minimum cell diameter is an important property in determining the extent of cell transmembrane migration into the pores and their subsequent migration to the other side of the porous film. The use of small-pore films might therefore prove advantageous in a graft to avoid the transmembrane transfer of different cell types.

Keratinocyte ultrastructure

Ultrastructure of individual keratinocytes grown on flat and porous films showed a 3- to 4-cell multi-layered but incompletely keratinized epidermis, typical of cells maintained in submerged culture (keratinocytes seeded on 5-μm film Fig. 4M, N). At the apical surface, there were numerous villus-like structures and linking adjacent keratinocytes. There were electron-dense desmosomal plaques associated with keratin intermediate-filament bundles (Fig. 4N, white arrow and inset). At the basal pole of the cultured epidermis, there were severely disorganized keratin filaments, but no basal lamina or well-formed hemidesmosome structures were present (Fig. 4M). Small, hypoplastic hemidesmosomes were occasionally observed along the basal pole but were not attached or associated with any external or underlying structures. Sub-basal dense plates were not observed on

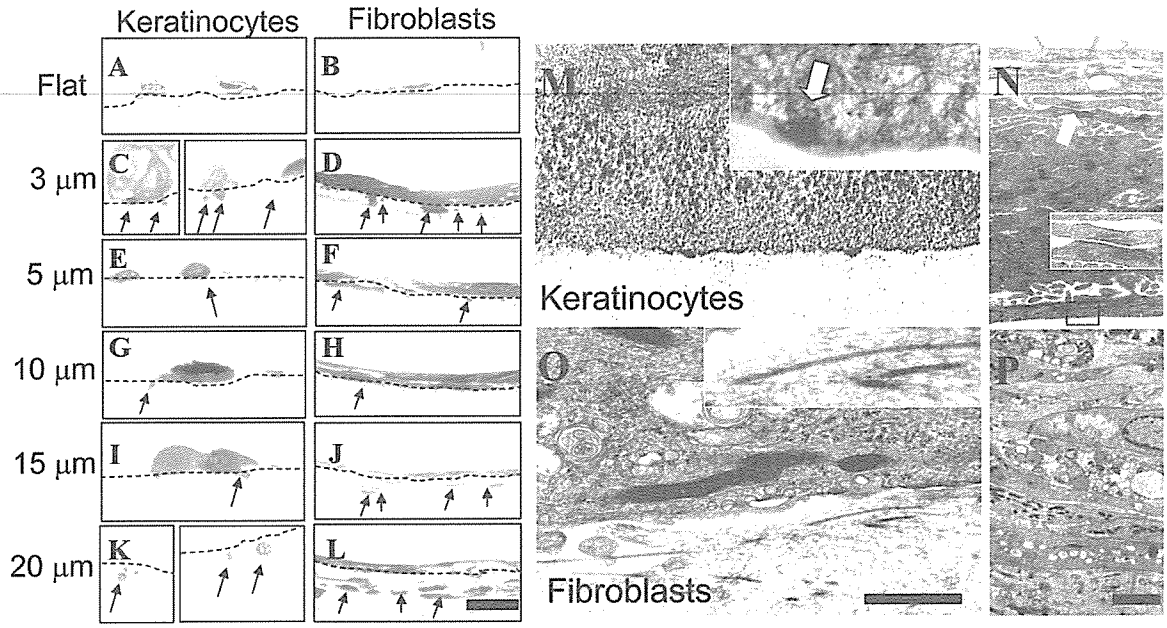

FIG. 4. Semithin and transmission electron microscopy shows the cell morphology, position, and ultrastructure of cells grown on porous films. The dotted lines (**A–J**) highlight the upper surfaces of the films. Both cell types grown on small-pore films (**A–D,** 3-5 μm, arrows) produced filopodial cell projections into the pore space. Furthermore, keratinocytes grown on larger pores (10- to 20-μm-sized pores, **E–J,** arrows) formed larger processes, and on the 20-μm pores, the keratinocytes entered the pore (see arrows in **I**). Often these isolated cells showed pyknotic nuclei and failed to survive (**I**). Fibroblasts were generally longer than even the largest pore size and entered pore sizes greater than 10 μm. The histology of keratinocyte (**H**) and fibroblast (**I**) long-term cultures maintained for 3 weeks shows multiple layers of cells. Ultrastructural analysis of keratinocytes showed no basal lamina or properly formed hemidesmosomes (**M,** arrows, inset in **M**). However, multiple intermediate and microfilaments were observed overlying the keratinocyte plasma membrane (**M, N**). Desmosomes were also seen between keratinocytes (white arrows in **N**, inset). Fibroblasts formed thin, elongated stacks of active cells containing vesicles and mitochondria and collagen fibers between adjacent cells. Scale bar 10 μm (**A–L**), 100 nm (**M, O**), 1 μm (**N, P**). Color images available online at www.liebertpub.com/ten.

any hemidesmosomes. A significant number of substratum-associated actin microfilament bundles were observed at the base of the basal layer keratinocytes (Fig. 4M) and in cell processes (data not shown).

Fibroblast ultrastructure

The ultrastructure of fibroblasts grown on 5-μm porous films showed heterogeneous layers of closely and loosely packed fibroblasts (Fig. 4O, P). Fibroblast morphology was generally that of active cells containing numerous secretory and endocytotic vesicles and together with numerous organelles (Fig. 4P). Cultured fibroblasts typically formed between 2 and 4 cell layers, in which the cells were closely packed or contained intercellular spaces filled with extracellular matrix, ground substance, and cross-banded collagen fibers (Fig. 4O, inset). A significant amount of substratum-associated actin microfilament and (presumably vimentin) intermediate filament bundles were observed within the fibroblasts (Fig. 4O) and in cell processes (data not shown).

Confocal fluorescence microscopy

Keratinocytes cultured on 3-μm films stained with keratin 14 and at the cell borders with the cell adhesion markers desmoplakin and E-cadherin. Keratinocytes showed bright staining for the focal contact and adhesion associated antigens vinculin, actin, and vitronectin but not for the epidermal matrix proteins or the hemidesmosomal anchoring filament protein laminins 5 (332), laminin 10/11 (511 or 521), collagen I, or collagen IV. Collagen VII and fibronectin showed weak epidermal cytoplasmic staining but no evidence of matrix deposition on the film.

Fibroblasts cultured on 5-μm films stained with vimentin (not keratin) and at the cell borders and extracellularly with fibronectin, vitronectin, and collagen I. Fibroblasts showed normal, bright cytoplasmic staining for the focal contact-associated antigens vinculin and actin and weaker staining for talin but no staining for the epidermal matrix proteins laminins 5(332), laminin 10 (511), collagen I, or collagen IV. Collagen VII showed weak cytoplasmic staining with no evidence of matrix deposition on the film.

DISCUSSION

Keratinocytes and fibroblasts adhere to, spread on, and can grow and survive on flat and all sizes of regular, hexagonally packed porous (ε-calprolactone) films with pores ranging in size from 3 to 20 μm. Specifically, we have demonstrated that keratinocyte attachment is dependent on the size of the pores and that cell adhesion was highest on the smallest 3-μm films. The unique characteristics of the porous patterned films account for these changes in the 2 cell types studied. Each cell type displays subtle differences due to their particular adhesion and growth characteristics, as shown by their unique repertoire of cell-adhesion receptors and cell–cell interactions with porous substrates.

Substrate characteristics, temperature, the presence of cations,[32] cell activation state, and cell viability, which is modulated by cytokines, govern keratinocyte adhesion in part. Keratinocytes in our study were more discriminating than fibroblasts and adhered best on smaller-pore-sized film (3-μm-pored films), the next best adhesion pore size being 5-μm-pore film. The explanation for these effects comes after several observations. First, if this pore size is greater than the size of the initial seeded cells, they can and do enter the film pores. Because keratinocytes require direct adjacent cell–cell contact for proper levels of growth, signaling, and cell survival, cell separation caused by the larger pores is likely to detrimentally affect these processes. It has previously been shown that keratinocytes seeded onto grafts without proper cell–cell and cell–substrate contact fail to form appropriate epidermal sheets[33] and survive in culture.[28,33] Further beneficial characteristics of the small-pore films include the fact that they have a greater surface area over which cells can adhere. Finally, the smaller pore size produces a greater length of pore edge per surface area that cells can insert their plasma membrane lamelapodia and filopodial extensions into to gain leverage and increase cell adhesion. This leverage may also inhibit cell migration. Keratinocytes require cell–cell and cell–substrate contact especially for cell growth and survival. When cells, especially keratinocytes, become isolated or removed from adjacent cell–cell contact (or are trapped in pores) readily undergo cell cycle arrest or apoptotic changes,[34] as was seen with pyknotic cells in our growth experiments. Similarly, mutations in the first human genetic disease affecting focal contact-adhesion protein kindlin-1 in skin also cause premature keratinocyte cell death by apoptosis and skin thinning and erosions.[35–37]

Our data suggest that the most important keratinocyte adhesive mechanism does not involve the proper formation of the hemidesmosome junction or the assembly of any extracellular components, including laminins 5/10[29] or matrix secretion of collagens I, IV, and VII. Conversely, fibroblasts and keratinocytes that adhered to porous films assembled highly dynamic, actin-associated focal adhesion-like structures that were observed attaching to the surface of the films. Given the short time frame over which cells, particularly fibroblasts, adhered to and spread on the films and taken together with the abundance of cytoplasmic actin filaments and focal adhesion components observed within filopodia and lamelapodia, we suggest that focal adhesions form the majority of adhesive junctions on these surfaces. The identification of fibronectin and vitronectin deposits in cultures and recent findings of the importance of focal contacts and their associated proteins on the adhesion of other cell types cultured on porous membranes further supports this hypothesis.[19,38,39]

Closely related to the film adhesive characteristics is the related ability to allow cell migration. The ability of the cells to gain leverage because of the extra length of pore edge or to enter the film pores in the small-pore samples probably affected keratinocyte and fibroblast migration rates, as previously mentioned. Our findings support previous reports that fibroblast migration on collagen sponges with various size pores was significantly greater than that of keratinocytes.[40]

In addition, we demonstrated that the smallest, 3-μm pore size was most efficient at inhibiting the transmigration of both cell types (to the opposite side of the film). Cell transmigration has important future implications in the design of monolayer or bilayer polymer grafts for the treatment of skin wounds. The beneficial adhesive properties and blocking of transmigration of the smaller pores will prove to be an important factor when this film is used to support a bilayered human skin equivalent or dermal equivalent by preventing two different cells types from mixing.

Keratinocytes are more selective than fibroblasts and grow best on small pore-sized film (3-μm-pored films). The second most effective film size for keratinocyte adhesion was the 5-μm film ($3\,\mu m > 5\,\mu m > 10\,\mu m >$ flat $>> 15\,\mu m < 20\,\mu m$). Explaining these growth effects on both cell types encompasses cell substrate adhesion and ability to migrate and form cell–cell contacts that all contributed to affect *in vitro* growth rates.[41] Our data suggested that the keratinocytes were more likely to grow poorly in isolation or in small colonies without significant all-round cell–cell contact. This would have important implications for cell contact–induced growth signals.[42,43] Other reports have also indicated that keratinocytes were more likely to grow poorly in isolation without cell–cell contact similar to that seen on porous collagen sponges.[40] Fibroblasts grew equally well on flat or small-pore-sized film but on pores larger than 10 μm showed significantly slower grow rates. Direct migration of fibroblasts on the underlying substrate was relatively short term due to formation of multiple cell layers. However, fibroblast adhesion and growth-signaling mechanisms are known to involve many of the same actin-associated focal-adhesion molecules as in keratinocytes.[44–46] NIH 3T3 fibroblasts have previously been demonstrated to adhere to all sizes of porous films.[24]

The important characteristics of porous films that cause significant changes in cell adhesion, migration, and growth rates include characteristics that enable cells to extend focal-contact plasma-membrane projections to gain adhesion and leverage that allow better growth. Further work is required to

describe the properties of PCL films with smaller pores and to determine whether further beneficial effects of adhesion, growth, and increases in keratinocyte migration rates that are observed in culture are maintained in *in vivo* wound-healing models.

ACKNOWLEDGMENTS

We thank Ms. Y. Miyamura and Ms. N. Ikeda for their excellent technical assistance in cell-film preparation, Mr. H. Nakamura and Ms. K. Sakai for their electron microscopy assistance, and Ms. Y. Morita and Ms. E. Ito for their excellent technical assistance in film fabrication and help with the migration studies. This work was supported by a grant-in-aid from the Health and Labor Sciences Research Grant (research into Human Genome, Tissue Engineering) H17-Saisei-12 (to J.R.M.) and by a grant-in-aid of Scientific Research A (17209038, H.S.) from the Japanese Society for the Promotion of Science. This work was also supported by a Health and Labor Sciences Research Grant (Research into Measures Treating Intractable Diseases) from the Ministry of Health, Labor and Welfare (H16-Nanchi-05, to H.S.) and a Project for Realization of Regenerative Medicine from the Ministry of Education, Science, Sports, and Culture of Japan (to H.S.). The hybridoma monoclonal antibody supernatants were obtained from the Developmental Studies Hybridoma Bank, developed under the auspices of the National Institute of Child Health and Development and maintained by the Department of Biological Sciences, University of Iowa, Iowa City, Iowa.

REFERENCES

1. Stenzel-Rosenbaum, M.H., Davis, T.P., Fane, A.G., and Chen, V. Porous polymer films and honeycomb structures made by the self-organization of well-defined macromolecular structures created by living radical polymerization techniques. Angew Chem Int Ed Engl **40,** 3428, 2001.
2. Zein, I., Hutmacher, D.W., Tan, K.C., and Teoh, S.H. Fused deposition modeling of novel scaffold architectures for tissue engineering applications. Biomaterials **23,** 1169, 2002.
3. Chung, T.W., Yang, M.G., Liu, D.Z., Chen, W.P., Pan, C.I., and Wang, S.S. Enhancing growth human endothelial cells on arg-gly-asp (RGD) embedded poly (epsilon-caprolactone) (PCL) surface with nanometer scale of surface disturbance. J Biomed Mater Res A **72,** 213, 2005.
4. Serrano, M.C., Pagani, R., Vallet-Regi, M., Pena, J., Ramila, A., Izquierdo, I., and Portoles, M.T. *In vitro* biocompatibility assessment of poly(epsilon-caprolactone) films using l929 mouse fibroblasts. Biomaterials **25,** 5603, 2004.
5. Ng, K.W., Khor, H.L., and Hutmacher, D.W. *In vitro* characterization of natural and synthetic dermal matrices cultured with human dermal fibroblasts. Biomaterials **25,** 2807, 2004.
6. Wake, M.C., Gupta, P.K., and Mikos, A.G. Fabrication of pliable biodegradable polymer foams to engineer soft tissues. Cell Transplant **5,** 465, 1996.
7. Wake, M.C., Patrick, C.W., Jr., and Mikos, A.G. Pore morphology effects on the fibrovascular tissue growth in porous polymer substrates. Cell Transplant **3,** 339, 1994.
8. Lee, S.J., Choi, J.S., Park, K.S., Khang, G., Lee, Y.M., and Lee, H.B. Response of mg63 osteoblast-like cells onto polycarbonate membrane surfaces with different micropore sizes. Biomaterials **25,** 4699, 2004.
9. Wan, Y., Wang, Y., Liu, Z., Qu, X., Han, B., Bei, J., and Wang, S. Adhesion and proliferation of oct-1 osteoblast-like cells on micro- and nano-scale topography structured poly(l-lactide). Biomaterials **26,** 4453, 2005.
10. Berry, C.C., Campbell, G., Spadiccino, A., Robertson, M., and Curtis, A.S. The influence of microscale topography on fibroblast attachment and motility. Biomaterials **25,** 5781, 2004.
11. O'Brien, F.J., Harley, B.A., Yannas, I.V., and Gibson, L.J. The effect of pore size on cell adhesion in collagen-gag scaffolds. Biomaterials **26,** 433, 2005.
12. Lee, S.H., Kim, B.S., Kim, S.H., Choi, S.W., Jeong, S.I., Kwon, I.K., Kang, S.W., Nikolovski, J., Mooney, D.J., Han, Y.K., and Kim, Y.H. Elastic biodegradable poly(glycolide-co-caprolactone) scaffold for tissue engineering. J Biomed Mater Res **66A,** 29, 2003.
13. Jeong, S.I., Kim, S.H., Kim, Y.H., Jung, Y., Kwon, J.H., Kim, B.S., and Lee, Y.M. Manufacture of elastic biodegradable plcl scaffolds for mechano-active vascular tissue engineering. J Biomater Sci Polym Ed **15,** 645, 2004.
14. Wald, H.L., Sarakinos, G., Lyman, M.D., Mikos, A.G., Vacanti, J.P., and Langer, R. Cell seeding in porous transplantation devices. Biomaterials **14,** 270, 1993.
15. Choi, Y.S., Hong, S.R., Lee, Y.M., Song, K.W., Park, M.H., and Nam, Y.S. Studies on gelatin-containing artificial skin: II. Preparation and characterization of cross-linked gelatin-hyaluronate sponge. J Biomed Mater Res **48,** 631, 1999.
16. Tanaka, M., Takebayashi, M., Miyama, M., Nishida, J., and Shimomura, M. Design of novel biointerfaces (II). Fabrication of self-organized porous polymer film with highly uniform pores. Biomed Mater Eng **14,** 439, 2004.
17. Saito, A., Taketani, S., Arai, K., Tanaka, M., Shimomura, M., and Sawa, Y. Highly regular honeycomb-patterned biodegradable scaffold promotes topographical control of myoblast proliferation and differentiation: A novel scaffold for myocardial regenerative therapy. J Mol Cell Cardiol **39,** 1022, 2005.
18. Tsuruma, A., Tanaka, M., Fukushima, N., and Shimomura, M. Morphological changes of neurons on self-organized honeycomb patterned films. Kobunshi Ronbunshu **61,** 628, 2004.
19. Tanaka, M., Tanakaya, A., Ito, E., Sunami, H., Yamamoto, S., and Shimomura, M. Effect of pore size of self-organized honeycomb-patterned polymer films on spreading, focal adhesion, proliferation, and function of endothelial cells. J Nanosci Nanotech in press.
20. Schwope, A.D., Wise, D.L., Sell, K.W., Dressler, D.P., and Skornick, W.A. Evaluation of wound-covering materials. J Biomed Mater Res **11,** 489, 1977.
21. Shimomura, M., Tanaka, M., Tsuruma, A., Sunami, H., and Yamamoto, S. Biomedical application of patterned polymer films prepared by self-organization. J Surf Sci Soc Jap **27,** 170, 2006.
22. Tsuruma, A., Tanaka, M., Fukushima, N., Yamamoto, S., and Shimomura, M. Morphological changes in neurons by self-organized patterned films. e-J Surf Sci Nanotech **3,** 159, 2005.

23. Tsuruma, A., Tanaka, M., Yamamoto, S., Fukushima, N., and Shimomura, M. Topographical control of neurites extension on stripe-patterned polymer films. Colloids Surf A Physicochem Eng Asp **284–285,** 548, 2006.
24. Fukuhira, Y., Kitazono, E., Hayashi, T., Kaneko, H., Tanaka, M., Shimomura, M., and Sumi, Y. Biodegradable honeycomb-patterned film composed of poly(lactic acid) and dioleoylphosphatidylethanolamine. Biomaterials **27,** 1797, 2006.
25. Yabu, H., Takebayashi, M., Tanaka, M., and Shimomura, M. Superhydrophobic and lipophobic properties of self-organized honeycomb and pincushion structures. Langmuir **21,** 3235, 2005.
26. Tanaka, Y., Sung, K.C., Tsutsumi, A., Ohba, S., Ueda, K., and Morrison, W.A. Tissue engineering skin flaps: which vascular carrier, arteriovenous shunt loop or arteriovenous bundle, has more potential for angiogenesis and tissue generation? Plast Reconstr Surg **112,** 1636, 2003.
27. Yabu, H., Tanaka, M., Ijiro, K., and Shimomura, M. Preparation of honeycomb-patterned polyimide films by self-organization. Langmuir **19,** 6297, 2003.
28. Butler, C.E., Orgill, D.P., Yannas, I.V., and Compton, C.C. Effect of keratinocyte seeding of collagen-glycosaminoglycan membranes on the regeneration of skin in a porcine model. Plast Reconstr Surg **101,** 1572, 1998.
29. McMillan, J.R., Akiyama, M., Nakamura, H., and Shimizu, H. Colocalization of multiple laminin isoforms predominantly beneath hemidesmosomes in the upper lamina densa of the epidermal basement membrane. J Histochem Cytochem **54,** 109, 2006.
30. Richardson, K.C., Jarret, L., and Finke, E.H. Embedding in epoxy resins for ultrathin sectioning in electron microscopy. Stain Technol **35,** 313, 1960.
31. Chometon, G., Zhang, Z.G., Rubinstein, E., Boucheix, C., Mauch, C., and Aumailley, M. Dissociation of the complex between cd151 and laminin-binding integrins permits migration of epithelial cells. Exp Cell Res 2006.
32. Patel, H., Marcelo, C., Voorhees, J.J., and Diaz, L.A. *In vitro* alterations of epidermal cell adhesion induced by temperature, substrate, and cations. J Invest Dermatol **76,** 474, 1981.
33. Rompre, P., Auger, F.A., Germain, L., Bouvard, V., Lopez Valle, C.A., Thibault, J., and Le Duy, A. Influence of initial collagen and cellular concentrations on the final surface area of dermal and skin equivalents: A Box-Behnken analysis. *In Vitro* Cell Dev Biol **26,** 983, 1990.
34. Presland, R.B., Kuechle, M.K., Lewis, S.P., Fleckman, P., and Dale, B.A. Regulated expression of human filaggrin in keratinocytes results in cytoskeletal disruption, loss of cell-cell adhesion, and cell cycle arrest. Exp Cell Res **270,** 199, 2001.
35. Lanschuetzer, C.M., Muss, W.H., Emberger, M., Pohla-Gubo, G., Klausegger, A., Bauer, J.W., and Hintner, H. Characteristic immunohistochemical and ultrastructural findings indicate that kindler's syndrome is an apoptotic skin disorder. J Cutan Pathol **30,** 553, 2003.
36. Jobard, F., Bouadjar, B., Caux, F., Hadj-Rabia, S., Has, C., Matsuda, F., Weissenbach, J., Lathrop, M., Prud'homme, J.F., and Fischer, J. Identification of mutations in a new gene encoding a FERM family protein with a pleckstrin homology domain in kindler syndrome. Hum Mol Genet **12,** 925, 2003.
37. Siegel, D.H., Ashton, G.H., Penagos, H.G., Lee, J.V., Feiler, H.S., Wilhelmsen, K.C., South, A.P., Smith, F.J., Prescott, A.R., Wessagowit, V., Oyama, N., Akiyama, M., Al Aboud, D., Al Aboud, K., Al Githami, A., Al Hawsawi, K., Al Ismaily, A., Al-Suwaid, R., Atherton, D.J., Caputo, R., Fine, J.D., Frieden, I.J., Fuchs, E., Haber, R.M., Harada, T., Kitajima, Y., Mallory, S.B., Ogawa, H., Sahin, S., Shimizu, H., Suga, Y., Tadini, G., Tsuchiya, K., Wiebe, C.B., Wojnarowska, F., Zaghloul, A.B., Hamada, T., Mallipeddi, R., Eady, R.A., McLean, W.H., McGrath, J.A., and Epstein, E.H. Loss of kindlin-1, a human homolog of the caenorhabditis elegans actin-extracellular-matrix linker protein unc-112, causes kindler syndrome. Am J Hum Genet **73,** 174, 2003.
38. Yamamoto, S., Tanaka, M., Sunami, H., Yamashita, S., Morita, Y., and Shimomura, M. Relationship between adsorbed fibronectin and cell adhesion on a honeycomb-patterned film. Surf Sci in press.
39. Yamamoto, S., Tanaka, M., Sunami, H., Yamashita, S., Morita, Y., and Shimomura, M. Relationship between adsorbed fibronectin and fak activation on a honeycomb-patterned film. J Surf Sci Soc Jap in press.
40. McKegney, M., Taggart, I., and Grant, M.H. The influence of crosslinking agents and diamines on the pore size, morphology and the biological stability of collagen sponges and their effect on cell penetration through the sponge matrix. J Mater Sci Mater Med **12,** 833, 2001.
41. Dai, N.T., Williamson, M.R., Khammo, N., Adams, E.F., and Coombes, A.G. Composite cell support membranes based on collagen and polycaprolactone for tissue engineering of skin. Biomaterials **25,** 4263, 2004.
42. Zhu, A.J. and Watt, F.M. Expression of a dominant negative cadherin mutant inhibits proliferation and stimulates terminal differentiation of human epidermal keratinocytes. J Cell Sci **109 (Pt 13),** 3013, 1996.
43. Takeichi, M., Watabe, M., Shibamoto, S., and Ito, F. Cadherin-dependent organization and disorganization of epithelial architecture. Princess Takamatsu Symp **24,** 28, 1994.
44. Akiyama, S.K., Larjava, H., and Yamada, K.M. Differences in the biosynthesis and localization of the fibronectin receptor in normal and transformed cultured human cells. Cancer Res **50,** 1601, 1990.
45. Kelly, T., Molony, L., and Burridge, K. Purification of two smooth muscle glycoproteins related to integrin. Distribution in cultured chicken embryo fibroblasts. J Biolog Chem **262,** 17189, 1987.
46. Srivastava, J., Elliott, B.E., Louvard, D., and Arpin, M. Src-dependent ezrin phosphorylation in adhesion-mediated signaling. Mol Biol Cell 2005.

Address reprint requests to:
James R. McMillan, M.Sc. Ph.D.
Department of Dermatology
Hokkaido University Graduate School of Medicine
North 15 West 7, Kitaku
Sapporo 060-8638, Japan

E-mail: jrm57@med.hokudai.ac.jp

ORIGINAL ARTICLE

DNA-Based Prenatal Diagnosis of Harlequin Ichthyosis and Characterization of *ABCA12* Mutation Consequences

Masashi Akiyama[1,5], Matthias Titeux[2,5], Kaori Sakai[1], James R. McMillan[1], Laure Tonasso[2], Patrick Calvas[3], Frederique Jossic[4], Alain Hovnanian[2,3] and Hiroshi Shimizu[1]

Until the identification of *ABCA12* as the causative gene, prenatal diagnosis (PD) for harlequin ichthyosis (HI) had been performed by electron microscopic observation of fetal skin biopsy samples. We report the first case of HI DNA-based PD. Direct sequence analysis of *ABCA12* revealed that the deceased proband was a compound heterozygote for two novel mutations. The maternal nonsense mutation p.Ser1249Term likely leads to nonsense-mediated messenger RNA decay. The paternal mutation c.7436G>A affects the last codon of exon 50 and was expected to be a splice site mutation. For their third pregnancy, the parents requested PD. Direct sequence analysis of fetal genomic DNA from amniotic fluid cells at 17 weeks gestation revealed the fetus was a compound heterozygote for both mutations. The parents requested the pregnancy to be terminated. Analysis of *ABCA12* transcripts of cultured keratinocytes from the abortus showed the presence of six abnormally spliced products from the allele carrying the splice site mutation. Four of them lead to premature termination codons whereas the two others produced shortened proteins missing 21 and 31 amino acids from the second ATP-binding cassette. This report provides evidence for residual ABCA12 expression in HI, and demonstrates the efficiency of early DNA-based PD of HI.

Journal of Investigative Dermatology (2007) **127,** 568–573. doi:10.1038/sj.jid.5700617; published online 2 November 2006

INTRODUCTION

Harlequin ichthyosis (HI) is a severe and usually fatal congenital ichthyosis with an autosomal recessive inheritance pattern (Williams and Elias, 1987; Akiyama, 2006). The clinical features include thick, plate-like scales with ectropion, eclabium, and flattened ears. Infants affected with HI frequently die within the first few weeks of life. Skin development is altered *in utero*; hyperkeratosis of the hair canal occurs in the second trimester and characteristic ultrastructural abnormalities including abnormal lamellar granules, are present in the affected fetal epidermis (Dale *et al.*, 1990; Akiyama *et al.*, 1994, 1998). Before the gene underlying HI was identified in 2005, prenatal diagnosis (PD) of the disease relied on ultrastructural examination of fetal skin biopsy samples at 19–23 weeks estimated gestational age (EGA) (Blanchet-Bardon *et al.*, 1983; Suzumori and Kanzaki, 1991; Akiyama *et al.*, 1994, 1999).

ABCA12 is a transporter which belongs to the ATP-binding cassette (ABC) transporter superfamily (Annilo *et al.*, 2002; Uitto, 2005). In 2005, we identified serious loss of function mutations in *ABCA12* coding an ABC transporter, that leads to defective lipid transport in epidermal keratinocytes and results in an HI phenotype (Akiyama *et al.*, 2005). Another group independently demonstrated that mutations in ABCA12 underlie HI by linkage analysis (Kelsell *et al.*, 2005). Thus, HI PD using molecular *ABCA12* mutational analysis has become possible. We report here the first successful DNA-based PD for HI using fetal genomic DNA specimens from amniotic fluid cells.

RESULTS

Case history and the clinical features of the proband

The newborn proband was the first child from unrelated, healthy French parents. He was affected with HI and died soon after birth. He displayed severe hyperkeratosis with fissures over his entire body, severe ectropion, and eclabium (Figure 1a–c). There was no family history of genodermatoses in the family. The parents had a healthy son, their second child. For their third pregnancy, the parents requested HI PD.

[1]*Department of Dermatology, Hokkaido University Graduate School of Medicine, Sapporo, Japan;* [2]*Inserm, U563 and University Paul Sabatier, Toulouse, France;* [3]*Department of Medical Genetics, Purpan Hospital, Toulouse, France and* [4]*Department of Fetopathology, Nantes Hospital, Nantes, France*

[5]*These authors contributed equally to this work*

Correspondence: Dr Masashi Akiyama, Department of Dermatology, Hokkaido University Graduate School of Medicine, North 15 West 7, Kita-ku, Sapporo 060-8638, Japan. E-mail: akiyama@med.hokudai.ac.jp

Abbreviations: ABC, ATP-binding cassette; cDNA, complementary DNA; EGA, estimated gestational age; HI, harlequin ichthyosis; HIK, HI keratinocytes; LG, lamellar granule; mRNA, messenger RNA; NHK, normal human keratinocytes; PD, prenatal diagnosis

Received 20 June 2006; revised 18 August 2006; accepted 19 September 2006; published online 2 November 2006

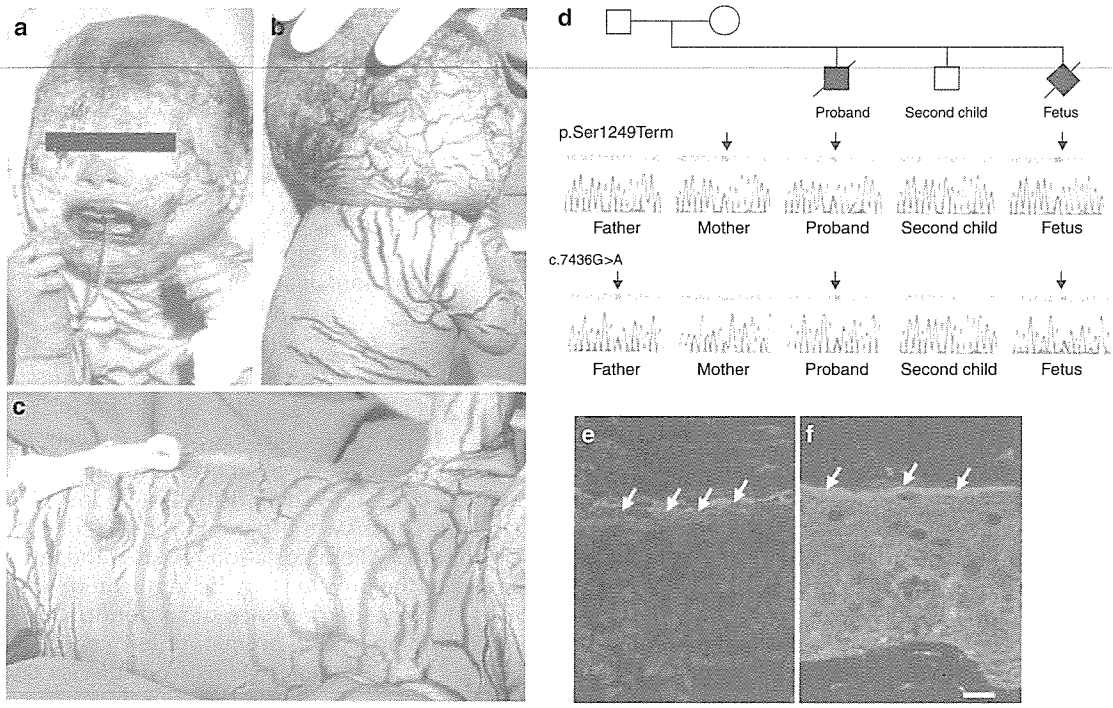

Figure 1. Clinical features of the proband, ABCA12 mutations in the family, and abnormal ABCA12 immunostaining in the patient's epidermis. (**a**, **b**, and **c**) Severe hyperkeratosis with fissures covering (**a**) the proband's face (**b**) scalp and back, (**c**) chest and abdomen. (**a**) Eclabium and (**b**) malformed pinna were apparent. (**d**) A novel nonsense mutation p.Ser1249Term was found in the proband, the mother, and the fetus (arrows). The novel splice site mutation c.7436G>A was detected in the proband, the father and the fetus (arrows). The fetus was prenatally diagnosed as affected. (**e**) In the patient's upper epidermis, weak ABCA12 immunostaining (green: arrows) was seen diffusely in the keratinocyte cytoplasm. (**f**) In normal control human epidermis, intense ABCA12 labeling (green) was noted in the granular layers (arrows). ABCA12, FITC (green); nuclear staining, propidium iodide (red). Bar = 10 μm.

ABCA12 mutation analysis

Mutation analysis of the 53 exons including the intron-exon boundaries of the entire *ABCA12* gene revealed that the proband was a compound heterozygote for two novel *ABCA12* mutations, c.3746C>A and c.7436G>A (sequence according to Lefèvre *et al.* (2003)) (GenBank accession NM 173076) (Figure 1d). c.3746C>A in exon 26 was a novel nonsense mutation that changed a serine residue at codon 1249 to a stop codon (p.Ser1249Term). This nonsense mutation p.Ser1249Term in exon 26 likely leads to nonsense-mediated messenger RNA (mRNA) decay rather than protein truncation, resulting in ABCA12 deficiency (see section *ABCA12* transcript analysis in cultured keratinocytes from the fetus). The mutation p.Ser1249Term was also found in the mother. The other mutation c.7436G>A in exon 50 affects the last amino acid of exon 50 and was expected to be a splice site mutation. Its potential effects on the splicing pattern of *ABCA12* pre-mRNA were investigated (see section *ABCA12* transcript analysis in cultured keratinocytes from the fetus). This splice site mutation was found in the father. Thus, the nonsense mutation p.Ser1249Term was of maternal origin and the splice site mutation c.7436G>A of paternal origin. These mutations were not found in 200 normal alleles (50 French and 50 Japanese healthy unrelated individuals) by sequence analysis, and were unlikely to be polymorphic variations (data not shown).

DNA-based PD of the fetus

Direct sequencing of PCR products including exon 26 or 50 of *ABCA12* from the fetal genomic DNA revealed the presence of the maternal nonsense mutation p.Ser1249Term in exon 26 and the paternal splice site mutation c.7436G>A in exon 50 (Figure 1d). Thus, the fetus harbored both *ABCA12* pathogenic mutations and was predicted to be affected. The pregnancy was terminated at 19 weeks gestation after the parents' request. The fetus showed characteristic changes including thin and fragile skin with petechia, eclabium, small, thickened and abnormally rimmed ears, rigid and swollen fingers and toes.

ABCA12 protein expression in the proband's skin

In the patient, ABCA12 immunostaining in the upper epidermis was reduced (Figure 1e), when compared with the intense ABCA12 immunostaining in the upper epidermal layers, mainly in the granular layers, of normal human skin (Figure 1f).

Ultrastructure of the skin from the abortus

Autopsy skin samples from the abortus showed abnormal, vacuolated lamellar granules in the upper intermediate cells and a large number of lipid droplets in the cytoplasm of incompletely keratinized keratinocytes.

ABCA12 transcript analysis in cultured keratinocytes from the fetus

Analysis of reverse transcription-PCR products from cultured keratinocytes of the fetus HI keratinocyte (HIK) and normal human keratinocytes (NHKs) on agarose gel electrophoresis revealed the presence of a single band in NHK PCR products and three bands in HIK PCR products (data not shown). PCR products were subsequently cloned and sequenced. A total of seven different mRNAs generated from the allele carrying the c.7436G>A mutation were identified (Figure 2a and b). Transcript p.Arg2479Lys corresponds to the full-length *ABCA12* transcript carrying a lysine residue in place of the arginine 2479. In addition, six of these transcripts are generated by splicing from several cryptic splice donor sites located in exon 50 of *ABCA12*. Transcript Δ4 carries a 4 bp deletion around the mutation (c.7433_7436del) leading to a frameshift and a PTC 11 amino acids downstream (p.Arg2479Leufs × 11). Transcript Δ31 displays a 31 bp deletion (c.7406_7436del) leading to a frameshift and a PTC 11 downstream (p.Ile2470_Arg2479>Leufs × 11). Transcript Δ43 presents a 43 bp deletion (c.7394_7436del) leading to a frameshift and a PTC 11 amino acids downstream (p.Lys2466_Arg2479>Leufs × 11). Transcript Δ50 shows a 50 bp deletion (c.7387_7436del) leading to a frameshift and a PTC 13 amino acids downstream (p.Asn2464_Arg2479>Trpfs × 13). Interestingly, transcript Δ63 predicts a truncated protein deleted from Leucine 2459 to Arginine 2479 (p.Leu2459_Arg2479del) owing to an in

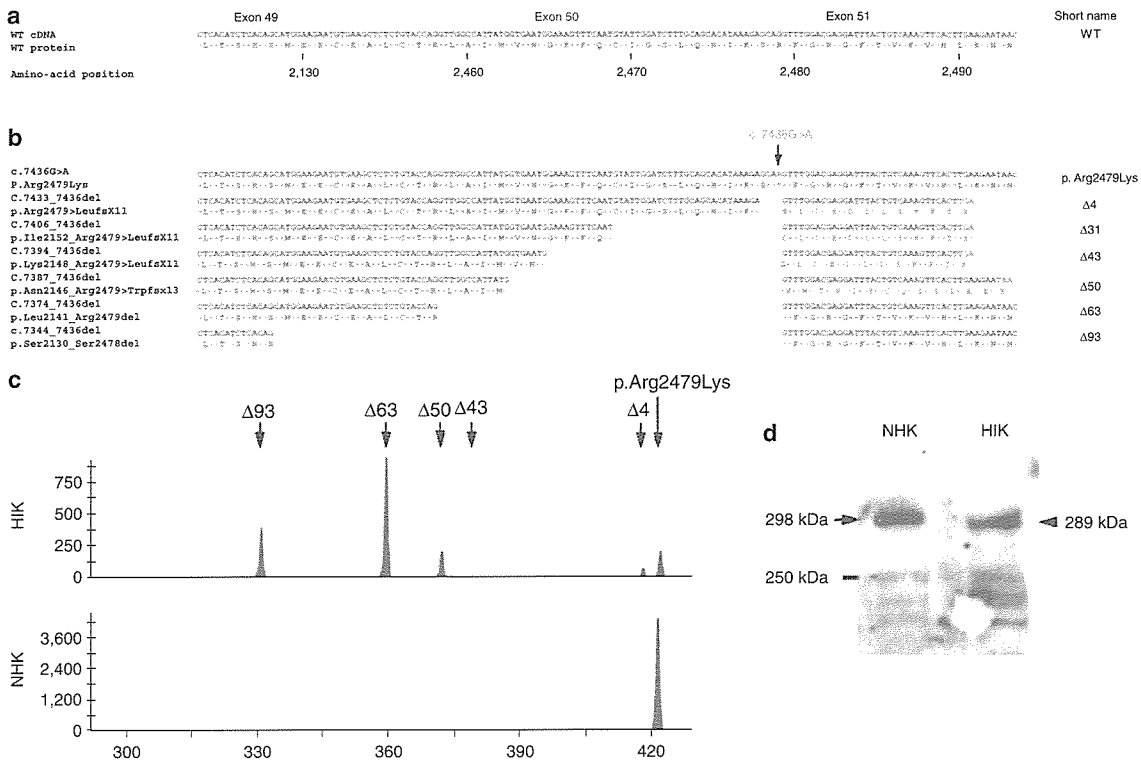

Figure 2. Expression analysis of ABCA12 transcripts and protein. (**a** and **b**) Sequence alignment of the several transcripts generated by the allele carrying the paternal splice site mutation c.7436G>A. (**a**) Wild-type cDNA (blue) and protein sequences of exon 50 of *ABCA12*. Amino-acid numbering is indicated. (**b**) Nucleotide and deduced protein sequences of splice variants of the allele carrying the c.7436G>A mutation (green). Premature stop codons and aberrant sequences owing to frameshifts are indicated in red. Splice variants include the correctly spliced product (p.Arg2479Lys) and six aberrantly spliced forms leading to out-of-frame (transcripts Δ4, Δ31, Δ43, and Δ50) and in-frame (Δ63 and Δ93) deletions. (**c**) Capillary electrophoresis analysis of *ABCA12* cDNA amplimers. Fragments extending over exons 49–53 were amplified by PCR using reverse-transcribed mRNA from primary cultures of HIK and NHKs. Although only one peak at 422 bp is present in NHK, several peaks are detected in HIK. The peak at 422 bp corresponds to the full-length transcript, arising either from the wild-type alleles (in NHK) or from the allele carrying the p.Ser1249Term null mutation and from the allele carrying the p.Arg2479Lys mutation (in HIK). The other peaks at 418, 379, 372, 359, and 329 bp, correspond respectively to transcripts Δ4, Δ43, Δ50, Δ63, and Δ93. The relative amount of each transcript, evaluated by the size of the peaks, shows that transcript Δ63 is predominant. Note that transcript Δ31 is missing, probably because its synthesis level is below the detection threshold of this technique. (**d**) Western blot analysis of ABCA12 protein in NHK and in HIK. A band at 298 kDa (arrow) is present in NHKs extract, however a slightly lower band (arrowhead, 289 kDa) is present in the HIK extracts. This lower band probably arises from the transcript Δ63 and to a less extent from the transcript Δ93.

frame deletion of 63 bp (c.7374_7436del), whereas transcript Δ93 presents an in frame skipping of the entire exon 50 predicting a truncated protein deleted from Serine 2448 to Serine 2478 (p.Ser2448_Ser2478del). The cryptic splice sites used to generate transcripts Δ4, Δ31, Δ50, and Δ63 were predicted using the automated splice site analysis software by Nalla and Rogan (2005).

Capillary electrophoresis analysis of the *ABCA12* complementary DNA (cDNA) amplimers showed one amplimer (422 bp) in NHKs corresponding to the normal sequence of exon 50, whereas five abnormal species were present in HIK (Figure 2c). All but one (Δ31) identified transcripts were found. The relative amount of transcript, indicated by the height of the peaks, showed that the Δ63 transcript is predominant, whereas the Δ31 transcript was not detectable. Interestingly, the height of the peak at 422 bp which arises from both the p.Arg2479Lys transcript and from the transcript synthesized from the other *ABCA12* allele carrying the p.Ser1249Term mutation is weak, indicating that the amount of both transcripts is low. This suggests that the allele carrying the null mutation is likely to be subjected to nonsense mediated mRNA decay and that only a small amount of ABCA12 protein arise from the natural splice site of the pre-mRNA carrying the c.7436G>A.

ABCA12 protein expression in fetal cultured keratinocytes

Western blot analysis revealed the presence of a band of an expected molecular weight of 298 kDa in protein extracts from NHKs, whereas a slightly smaller band of 289 kDa was seen in HI keratinocyte extracts (Figure 2d). This band probably corresponds to the proteins synthesized from both transcript Δ63 and transcript Δ93 which are predicted to encode proteins of calculated molecular weight of 291 and 289 kDa, respectively, and cannot be resolved on the SDS-PAGE. Smaller bands were seen in both extracts and probably correspond to degradation products. Western blot analysis failed to reveal the presence of other shortened proteins in the extract of HIK. However, the epitope recognized by the antibody is located at the end of the C-terminus domain of ABCA12 and thus is not present in the predicted proteins encoded by transcripts Δ4, Δ31, Δ43, and Δ50, and by the product of the allele carrying the p.Ser1249Term mutation.

DISCUSSION

HI is the most severe ichthyotic genodermatosis and has a very poor prognosis. Therefore, any parents' request for PD should be taken very seriously. However, until 2005 the causative gene had not been identified and previous prenatal diagnoses were performed using electron microscopic examination of fetal skin biopsies during the later stages of pregnancies (Blanchet-Bardon *et al.*, 1983; Suzumori and Kanzaki, 1991; Akiyama *et al.*, 1994, 1999). HI PD by fetal skin biopsy was usually performed at 21–22 weeks EGA (Blanchet-Bardon *et al.*, 1983; Suzumori and Kanzaki, 1991; Akiyama *et al.*, 1994, 1999). According to these reports, fetal skin biopsy specimens at that age showed characteristic abnormalities including a large number of lipid droplets in the keratinized cells and abnormal or absent lamellar granules, which were sufficient findings for the PD of the disorder.

However, PD of HI by fetal skin biopsy is technically difficult, requires excellent skin biopsy site selection, and is time-consuming. We need to gain a significant better understanding of fetal skin development and only a few experts are able to make this reliable diagnosis. Owing to the fact that the interfollicular epidermis at 19 weeks EGA or earlier is not sufficiently developed to exhibit the characteristic morphologic changes of keratinization (Holbrook and Odland, 1980), the observations of interfollicular keratinocytes are thought to sometime provide insufficient or unreliable information for PD or prenatal exclusion of HI. However, at 19 weeks EGA, we were able to see characteristic ultrastructural HI abnormalities in the keratinized cells in the hair canal or infundibulum of the developing hair follicle in the case of an affected fetus (Akiyama *et al.*, 1999). This is because keratinization in the hair cone and hair canal occurs at around 15 weeks EGA, approximately 8–9 weeks before the keratinization of interfollicular epidermis in human fetal skin development (Holbrook and Odland, 1978). However, fetal biopsy specimens at 19 weeks EGA may not always provide sufficient information for PD or exclusion of HI because the interfollicular epidermis has not yet keratinized at this stage of epidermal development (Shimizu *et al.*, 2005).

In 2005, *ABCA12* was identified as the underlying gene causing HI (Akiyama *et al.*, 2005; Kelsell *et al.*, 2005). Additional HI cases harboring *ABCA12* mutations have now been reported (Akiyama *et al.*, 2006a, b). Owing to these discoveries, it has now become possible to undertake HI DNA-based PD by chorionic villus or amniotic fluid sampling from the earlier stages of pregnancy. These procedures are technically more reliable and have a reduced burden on the mothers, as in other severe genetic keratinization disorders (Tsuji-Abe *et al.*, 2004). We report here a successful PD of HI using fetal genomic DNA obtained at 17 weeks EGA. It is anticipated that in the future, even earlier prenatal diagnoses using completely non-invasive analysis of DNA from fetal cells in the maternal circulation will be possible (Uitto *et al.*, 2003), as well as pre-implantation genetic diagnosis for HI (Shimizu and Suzumori, 1999).

Expression analysis of *ABCA12* in cultured keratinoctyes from the abortus revealed that the allele carrying the c.7436G>A mutation produced seven different transcripts. The synthesis of six different truncated or deleted transcripts from this allele explains the loss of function of this allele. In particular, transcripts Δ63 and Δ93 predict the synthesis of deleted proteins (deletion of 21 and 31 amino-acid residues, respectively) with calculated molecular weights of 291 and 289 kDa, which cannot be separated on the SDS-PAGE. Thus, the protein detected at 289 kDa is likely to arise from both transcripts, but predominantly from transcript Δ63, which is present in higher amount. The two proteins lack part of the second ATP-binding cassette, which is predicted to dramatically affect ABCA12 function. Although, small amounts of a full-length ABCA12 protein carrying the p.Arg2479Lys mutation may theoretically be synthesized, they were not

detected. Thus, loss of ABCA12 function results from the combination of a null allele, and the synthesis of non-functional deleted proteins unable to restore a normal phenotype.

The terminated fetuses in the previous reports of positive PD of HI showed macroscopic changes consistent with the HI phenotype at 22 weeks or older EGA (Blanchet-Bardon *et al.*, 1983; Suzumori and Kanzaki, 1991; Akiyama *et al.*, 1994, 1999). In our previous report, we demonstrated that an affected fetus already showed a clinically apparent HI phenotype at 21 weeks EGA (Akiyama *et al.*, 1999). Characteristic HI changes of HI were seen both macroscopically and ultrastructurally at 19 weeks EGA and the present case suggests that the HI phenotype has started to emerge in the affected fetus at the late second trimester of pregnancy.

MATERIALS AND METHODS

Mutation detection

Mutational analysis was performed in the proband and both parents. Briefly, genomic DNA isolated from peripheral blood was subjected to PCR amplification, followed by direct automated sequencing using an ABI PRISM 3100 genetic analyzer (ABI Advanced Biotechnologies, Columbia, MD). Oligonucleotide primers and PCR conditions used for amplification of all exons 1–53 of *ABCA12* were originally derived from the report by Lefèvre *et al.* (2003) and were partially modified as described previously (Akiyama *et al.*, 2005). The entire coding region including the exon/intron boundaries for both forward and reverse strands from the proband, the parents and 100 healthy control individuals (50 French and 50 Japanese) were sequenced.

DNA-based prenatal testing

Amniotic fluid cells were obtained under ultrasound guidance at 17 weeks gestation. Fetal DNA was extracted from fresh cells, and detection of *ABCA12* mutations targeting the mutations that were found in the proband was subsequently performed, as described above. There were no sonographic findings suggestive of an affected fetus. No complications arose from the procedure.

Cell culture

Primary human keratinocytes and fibroblasts were obtained from skin fragments of the abortus and a punch biopsy of a healthy control. Keratinocytes were cultured on a feeder layer of lethaly irradiated mouse 3T3-J2 fibroblasts as described previously (Barrandon and Green, 1987). Fibroblasts were grown in DMEM supplemented with 10% heat-inactivated fetal calf serum (Eurobio, Les Ulis, France).

RNA extraction and reverse transcription-PCR analysis

RNA from cultured keratinocytes and fibroblasts was extracted with the SV Total RNA Isolation System (Promega, Charbonnières, France), and first-strand cDNA synthesis was carried out using random hexamer primers and superscript II reverse transcriptase (Invitrogen, Carlsbad, CA). Next, a segment of the *ABCA12* cDNA was PCR-amplified with primers 5′-TCCGTCATCCTCACATCTTCA-3′ (forward) and 5′-GAACCTTGGCTGCTGGTATC-3′ (reverse) using Go-Taq polymerase (Promega, Charbonnières, France). The cDNA amplimers were cloned into PGEM-T vector (Promega, Charbonnières, France) and sequenced using the SP6 primer (5′-ATTTAGGT GACACTATAGAATAC-3′) and the T7 primer (5′-GTAATACGACT CACTATAGGGC-3′). In parallel, the cDNA amplimers were analyzed on standard agarose gel and by capillary electrophoresis on an ABI 310 Genetic Analyzer running the GeneScan software (Applied Biosystems, Foster City, CA).

Immunohistological and immunoblot analysis of ABCA12 protein expression

Immunodetection of ABCA12 was performed using an affinity purified anti-ABCA12 serum raised in rabbits using a 14 amino-acid sequence synthetic peptide (residues 2,567–2,580) derived from the ABCA12 sequence (NM 173076) as the immunogen (Akiyama *et al.*, 2005). Immunofluorescent labeling was performed as described previously (Akiyama *et al.*, 2000). Briefly, 6-μm-thick sections of fresh patient's skin were cut using a cryostat. The sections were incubated in primary antibody solution, anti-ABCA12 antiserum diluted 1/10, for 1 hour at 37°C. The sections were then incubated in FITC-conjugated goat anti-rabbit Igs diluted 1:100 (DAKO, Glostrup, Denmark) for 30 minutes at room temperature, followed by nuclear counterstain by propidium iodide (Sigma Chemical Co., St Louis, MO). The sections were extensively washed with phosphate-buffered saline between incubations. The stained sections were then mounted with a coverslip and observed using a confocal laser scanning microscope. For Western blot analysis, proteins were extracted from cultured keratinocytes in the presence of protease inhibitors (Complete Mini Protease Inhibitor Cocktail, Roche Diagnostics, Meylan, France), fractionated by SDS-PAGE using 30 μg/lane protein on a 4% gel, and transferred to a nitrocellulose membrane (Hybond-C Extra, Amersham Biosciences, Saclay, France). Membrane blocking and incubation with antibody (1:5,000) were carried out in phosphate-buffered saline with 5% skim milk. Secondary antibody was goat anti-rabbit IgG antibodies conjugated to horseradish peroxidase (1:5000, Cell Signalling Technology, Beverley). Signals were revealed with ECL + chemiluminescence reagents (GE Healthcare Bio-Sciences Corp., Piscataway, NJ).

Informed consent was obtained from the patients' parents. This study was approved by the medical ethical committees at the Hokkaido University, Sapporo, Japan, Purpan Hospital, Toulouse, France and Nantes University Hospital, Nantes, France. The study was conducted according to the Declaration of Helsinki Principles.

CONFLICT OF INTEREST

The authors state no conflict of interest.

ACKNOWLEDGMENTS

We thank Ms Megumi Sato, Ms Akari Nagasaki, and Ms Anne-Marie Mazarguil for their technical assistance on this project. This work was supported in part by The GENESKIN European project, the French Ministry of Health (Reference center for orphan skin diseases), Grants-in-Aid from the Ministry of Education, Science, Sports, and Culture of Japan to M. Akiyama (Kiban B. 16390312 and Kiban B. 18390310).

REFERENCES

Akiyama M (2006) Pathomechanisms of harlequin ichthyosis and ABCA transporters in human diseases. *Arch Dermatol* 142:914–8

Akiyama M, Dale BA, Smith LT, Shimizu H, Holbrook KA (1998) Regional difference in expression of characteristic abnormality of harlequin ichthyosis in affected fetuses. *Prenat Diagn* 18:425–36

Akiyama M, Kim D-K, Main DM, Otto CE, Holbrook KA (1994) Characteristic morphologic abnormality of harlequin ichthyosis detected in amniotic fluid cells. *J Invest Dermatol* 102:210–3

Akiyama M, Sakai K, Sugiyama-Nakagiri Y, Yamanaka Y, McMillan JR, Sawamura D *et al.* (2006a) Compound heterozygous mutations including a *de novo* missense mutation in *ABCA12* led to a case of harlequin ichthyosis with moderate clinical severity. *J Invest Dermatol* 126:1518–23

Akiyama M, Sakai K, Wolff G, Hausser I, McMillan JR, Sawamura D *et al.* (2006b) A novel ABCA12 mutation 3270delT causes harlequin ichthyosis. *Br J Dermatol* 155:1064–6

Akiyama M, Smith LT, Shimizu H (2000) Changing patterns of localization of putative stem cells in developing human hair follicles. *J Invest Dermatol* 114:321–7

Akiyama M, Sugiyama-Nakagiri Y, Sakai K, McMillan JR, Goto M, Arita K *et al.* (2005) Mutations in ABCA12 in harlequin ichthyosis and functional rescue by corrective gene transfer. *J Clin Invest* 115:1777–84

Akiyama M, Suzumori K, Shimizu H (1999) Prenatal diagnosis of harlequin ichthyosis by the examinations of keratinized hair canals and amniotic fluid cells at 19 weeks' estimated gestational age. *Prenat Diagn* 19:167–71

Annilo T, Shulenin S, Chen ZQ, Arnould I, Prades C, Lemoine C *et al.* (2002) Identification and characterization of a novel ABCA subfamily member, ABCA12, located in the lamellar ichthyosis region on 2q34. *Cytogenet Genome Res* 98:166–9

Barrandon Y, Green H (1987) Cell migration is essential for sustained growth of keratinocyte colonies: the roles of transforming growth factor-alpha and epidermal growth factor. *Cell* 50:1131–7

Blanchet-Bardon C, Dumez YFL, Lutzner MA, Puissant A, Henrion R, Bernheim A (1983) Prenatal diagnosis of harlequin fetus. *Lancet* 1:132

Dale BA, Holbrook KA, Fleckman P, Kimball JR, Brumbaugh S, Sybert VP (1990) Heterogeneity in harlequin ichthyosis, an inborn error of epidermal keratinization: variable morphology and structural protein expression and a defect in lamellar granules. *J Invest Dermatol* 94:6–18

Holbrook KA, Odland GF (1978) Structure of the human fetal hair canal and initial hair eruption. *J Invest Dermatol* 71:385–90

Holbrook KA, Odland GF (1980) Regional development of the human epidermis in the first trimester embryo and the second trimester fetus (ages related to the timing of amniocentesis and fetal biopsy). *J Invest Dermatol* 74:161–8

Kelsell DP, Norgett EE, Unsworth H, Teh M-T, Cullup T, Mein CA *et al.* (2005) Mutations in ABCA12 underlie the severe congenital skin disease harlequin ichthyosis. *Am J Hum Genet* 76:794–803

Lefèvre C, Audebert S, Jobard F, Bouadjar B, Lakhdar H, Boughdene-Stambouli O *et al.* (2003) Mutations in the transporter ABCA12 are associated with lamellar ichthyosis type 2. *Hum Mol Genet* 12: 2369–78

Nalla VK, Rogan PK (2005) Automated splicing mutation analysis by information theory. *Hum Mutat* 25:334–42

Shimizu A, Akiyama M, Ishiko A, Yoshiike T, Suzumori K, Shimizu H (2005) Prenatal exclusion of harlequin ichthyosis; potential pitfalls in the timing of the fetal skin biopsy. *Br J Dermatol* 153:811–4

Shimizu H, Suzumori K (1999) Prenatal diagnosis as a text for genodermatoses: its past, present and future. *J Dermatol Sci* 19:1–8

Suzumori K, Kanzaki T (1991) Prenatal diagnosis of harlequin ichthyosis by fetal skin biopsy; report of two cases. *Prenat Diagn* 11:451–7

Tsuji-Abe Y, Akiyama M, Nakamura H, Takizawa Y, Sawamura D, Matsunaga K *et al.* (2004) DNA-based prenatal exclusion of bullous congenital ichthyosiform erythroderma at the early stage, 10-11 weeks' of pregnancy in two consequent siblings. *J Am Acad Dermatol* 51:1008–11

Uitto J (2005) The gene family of ABC transporters – novel mutations, new phenotypes. *Trends Mol Med* 11:341–3

Uitto J, Pfendner E, Jackson LG (2003) Probing the fetal genome: progress in non-invasive prenatal diagnosis. *Trends Mol Med* 9:339–43

Williams ML, Elias PM (1987) Genetically transmitted, generalized disorders of cornification; the ichthyoses. *Dermatol Clin* 5:155–78

Gene Corner

A novel *ABCA12* mutation 3270delT causes harlequin ichthyosis

DOI: 10.1111/j.1365-2133.2006.07434.x

Harlequin ichthyosis (HI) is a severe and often fatal congenital ichthyosis with an autosomal recessive inheritance pattern.[1] The clinical features include thick, plate-like scales with ectropion, eclabium, and flattened ears. The skin development is altered *in utero*.[2] *ABCA12* mutations have been reported to underlie HI[3,4] and it was clarified that HI is caused by severe functional defects in the keratinocyte lipid transporter ABCA12.[3] The pathomechanism of HI lies in the defective function of the lipid transporter ABCA12 which causes abnormal lipid lamellar granule transport in the keratinocytes, and results in a malformation of the epidermal lipid barrier.[3] Until the 1980s, newborns affected with HI rarely survived beyond the neonatal period. However, recently, HI babies have often had a better prognosis.[5–7] It is still unclear whether the good prognosis in HI is due to some remnant ABCA12 protein transporter function in the patients or not. Here, we report a girl with HI with a novel homozygous *ABCA12* deletion mutation leading to a complete loss of function of ABCA12, who has survived despite having severe ichthyosis showing the clinical features of nonbullous congenital ichthyosiform erythroderma (NBCIE).

Case and methods

The patient is the first child of healthy, unrelated German parents. There was no positive family history of any related disorders. The baby girl was born after premature rupture of the amnion in the 34th week of pregnancy (weight 1930 g, length 43 cm, head circumference 32 cm). The skin of the newborn was covered with large, thick, white, diamond-shaped plaques, partly bordered by irregular, bleeding fissures (Fig. 1). Hands and feet were oedematous, the tips of the fingers and toes were white with tight skin, and mobility in all joints was reduced.

After therapy with oral retinoids and local application of carbamide and emollient ointment, in a humid incubator, the hyperkeratosis detached within 2–6 weeks and passive and spontaneous mobility increased. The oedema and skin tightness also decreased. During infancy, the patient showed white to grey scales on her erythematous trunk skin, extremities and face (Fig. 2). Now, at age 8 years, she is doing well with continuous therapy with emollient ointment, vitamin D_3 and iodide and the avoidance of sunlight, although she still has severe ichthyosis with several features of NBCIE. Her mental status is normal, and she attends the second grade of a normal school. At age 8 years the patient is 114 cm tall (below third percentile), demonstrating that growth development is delayed.

Mutational analysis of *ABCA12* was performed in the affected baby, her parents and her healthy sisters. Briefly, genomic DNA isolated from peripheral blood cells was subjected to polymerase chain reaction (PCR) amplification, followed by direct automated sequencing using an ABI PRISM 3100 Genetic Analyzer (ABI Advanced Biotechnologies, Columbia, MD, U.S.A.). Oligonucleotide primers and PCR conditions used for amplification of all exons 1–53 of *ABCA12* were originally derived from the report by Lefèvre *et al.*[8] and were partially modified for the present study. The entire coding region including the exon/intron boundaries for both forward and reverse strands from the patient, family members and 100 healthy controls was sequenced.

Biopsy samples from the patient's ichthyotic skin were fixed in 5% glutaraldehyde solution, postfixed in 1% OsO_4, dehydrated, and embedded in Epon 812. The samples were sectioned at 1 μm thickness for light microscopy and thin sectioned for electron microscopy (70 nm thick). The thin sections were stained with uranyl acetate and lead citrate and examined in a transmission electron microscope.

Results and discussion

Mutation analysis of the 53 exons including the exon/intron boundaries of the entire *ABCA12* gene revealed a homozygous deletion mutation 3270delT in exon 23 in the patient (sequence according to Lefèvre *et al.*;[8] GenBank NM173076; Fig. 3). The mutation was verified as present in a heterozygous fashion in her parents and a sister (Fig. 3). Another sister carried no mutations. The mutation was not found in sequence analysis of 200 alleles from 100 normal, unrelated individuals, and therefore is unlikely to be a polymorphism (data not shown). The deletion mutation 3270delT leads to a frameshift and introduces a stop codon at codon 1090, within the first transmembrane domain complex of the ABCA12 protein.[9] Thus, the homozygous deletion mutation results in a truncation of ABCA12 peptide with the loss of both ATP-binding cassettes (ABCs), and is thought to have a serious effect on the function of the ABCA12 protein.

Skin biopsy showed compact, severe hyperkeratosis. Electron microscopy revealed numerous abnormal lamellar

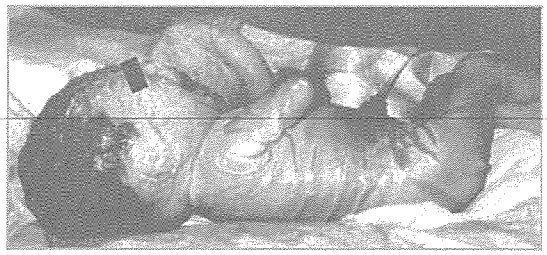

Fig 1. The patient showed the typical clinical phenotype of harlequin ichthyosis in the neonatal period. The entire body surface was covered with thick plate-like scales and fissures. Her auricles were malformed.

granules in the granular layer keratinocytes and accumulation of extruded irregular lamellar granules as vesicular structures, either empty or filled with glycogen-like particles between the epidermal cornified cells.

The ABC transporter superfamily is one of the largest gene families, encoding a highly conserved group of proteins involved in energy-dependent (active) transport of a variety of substrates across membranes.[10,11] The ABCA subfamily, of which the *ABCA12* gene is a member, is assumed to be involved in lipid transport.[12] Mutations in these genes underlie several human genetic diseases.[7,13] In 2005 it was reported that *ABCA12* mutations underlie HI,[3,4] and we showed that serious *ABCA12* mutations cause abnormal lipid transport via lamellar granules in keratinocytes, resulting in the malformation or improper assembly of the epidermal keratinocyte surface lipid barrier and the HI phenotype.[3] Recently, the long-term survival of patients with HI has been more frequently observed and documented,[3–7,14] despite HI having been considered to be an almost invariably fatal disorder until as recently as the 1980s. In the present patient with HI, the underlying *ABCA12* mutation, 3270delT, results in the truncation of the ABCA12 peptide at codon 1090 within the first transmembrane domain complex. Thus, the causative mutation leads to a loss of both ABCs and is thought to lead to a loss of ABCA12 function. Therefore, our homozygous patient is predicted to have an absence of ABCA12 transporter activity. However, our patient survived beyond the perinatal and neonatal period, probably in part due to the oral retinoid treatment. She is now 8 years old and her general condition is good without the need for retinoid treatment, although she

Fig 2. Clinical features at 3 years of age. The entire skin surface (A) was erythematous and covered with grey-white to grey scales, including the hands (B) and feet (C).

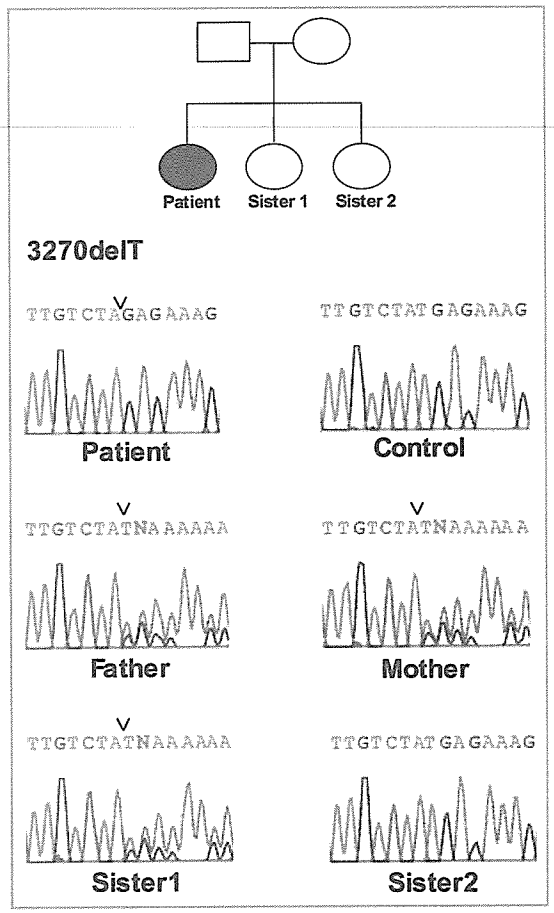

Fig 3. Homozygous mutation of *ABCA12* in the patient. The pedigree of the patient's family (top). Direct sequencing revealed a homozygous 3270delT (changing tyrosine residue at codon 1090 to a stop codon) in exon 23 of *ABCA12* of the patient. In both parents and one sister, the deletion mutation was found in a heterozygous state. The mutation was not present in the other sister or in the control samples.

has the clinical features of NBCIE over her entire body. This case may suggest that a patient with HI can survive beyond the perinatal and neonatal period with oral retinoid treatment, even if the causative *ABCA12* mutation leads to a complete loss of function of ABCA12. Further accumulation of similar cases is needed to confirm the effect of systemic retinoid on the prognosis of HI.

Acknowledgments

We thank Ms Maki Goto and Ms Akari Nagasaki for their fine technical assistance on this project. This work was supported in part by Grant-in-Aid from the Ministry of Education, Science, Sports, and Culture of Japan to M.A. (Kiban B 16390312 and Kiban B 18390310).

Department of Dermatology, Hokkaido University Graduate School of Medicine, North 15 West 7, Kita-ku, Sapporo 060-8638, Japan — M. Akiyama
Institut für Humangenetik und Anthropologie, Albert-Ludwigs-Universität Freiburg, Freiburg, Germany — K. Sakai, G. Wolff
†Department of Dermatology, University Clinic Heidelberg, Heidelberg, Germany — I. Hausser†
‡Creative Research Institute Sousei, Hokkaido University, Sapporo, Japan — J.R. McMillan‡, D. Sawamura, H. Shimizu
E-mail: akiyama@med.hokudai.ac.jp

References

1 Akiyama M. Harlequin ichthyosis and other autosomal recessive congenital ichthyoses: the underlying genetic defects and pathomechanisms. *J Dermatol Sci* 2006; **42**:83–9.
2 Akiyama M, Dale BA, Smith LT *et al.* Regional difference in expression of characteristic abnormality of harlequin ichthyosis in affected fetuses. *Prenat Diagn* 1998; **18**:425–36.
3 Akiyama M, Sugiyama-Nakagiri Y, Sakai K *et al.* Mutations in *ABCA12* in harlequin ichthyosis and functional rescue by corrective gene transfer. *J Clin Invest* 2005; **115**:1777–84.
4 Kelsell DP, Norgett EE, Unsworth H *et al.* Mutations in *ABCA12* underlie the severe congenital skin disease harlequin ichthyosis. *Am J Hum Genet* 2005; **76**:794–803.
5 Elias PM, Fartasch M, Crumrine D *et al.* Origin of the corneocyte lipid envelope (CLE): observations in harlequin ichthyosis and cultured human keratinocytes. *J Invest Dermatol* 2000; **115**:765–9.
6 Singh S, Bhura M, Maheshwari A *et al.* Successful treatment of harlequin ichthyosis with acitretin. *Int J Dermatol* 2001; **40**:472–3.
7 Akiyama M. Pathomechanisms of harlequin ichthyosis and ABC transporters in human diseases. *Arch Dermatol* (in press).
8 Lefèvre C, Audebert S, Jobard F *et al.* Mutations in the transporter *ABCA12* are associated with lamellar ichthyosis type 2. *Hum Mol Genet* 2003; **12**:2369–78.
9 Annilo T, Shulenin S, Chen ZQ *et al.* Identification and characterization of a novel ABCA subfamily member, *ABCA12*, located in the lamellar ichthyosis region on 2q34. *Cytogenet Genome Res* 2002; **98**:169–76.
10 Borst P, Elferink RO. Mammalian ABC transporters in health and disease. *Annu Rev Biochem* 2002; **71**:537–92.
11 Uitto J. The gene family of ABC transporters – novel mutations, new phenotypes. *Trends Mol Med* 2005; **11**:341–3.
12 Peelman F, Labeur C, Vanloo B *et al.* Characterization of the ABCA transporter subfamily: identification of prokaryotic and eukaryotic members, phylogeny and topology. *J Mol Biol* 2003; **325**:259–74.
13 Klein I, Sarkadi B, Varadi A. An inventory of the human ABC proteins. *Biochim Biophys Acta* 1999; **1461**:237–62.
14 Akiyama M, Sakai K, Sugiyama-Nakagiri Y *et al.* Compound heterozygous mutations including a *de novo* missense mutation in *ABCA12* led to a case of harlequin ichthyosis with moderate clinical severity. *J Invest Dermatol* 2006; **126**:1518–23.

Accepted for publication 3 May 2006

Key words: ABCA12 mutation, *ATP-binding cassette transporter, harlequin ichthyosis, lipid transporter, retinoid, truncation*

Conflicts of interest: None declared.

Arch Dermatol Res (2007) 298:403–407
DOI 10.1007/s00403-006-0702-0

SHORT COMMUNICATION

N-Linked neutral oligosaccharides in the stratum corneum of normal and ichthyotic skin

Hiroko Ito · Masashi Akiyama · Hiroaki Nakagawa · Rie Uematsu · Kisaburo Deguchi · James R. McMillan · Shin-Ichiro Nishimura · Hiroshi Shimizu

Received: 1 May 2006 / Revised: 23 August 2006 / Accepted: 28 August 2006 / Published online: 26 September 2006

Abstract *N*-Glycan oligosaccharides are thought to play multiple, important roles in a variety of biological events. However, *N*-glycan profiles in the stratum corneum of human skin have not yet been studied in detail. To clarify the *N*-glycan profiles in the stratum corneum of normal and ichthyotic epidermis, *N*-glycan profiles were studied by high-performance liquid chromatography using normal human epidermal samples and scales from hyperkeratotic skin of ichthyosis patients. Chromatograms of patient scale samples showed unique alterations in three peaks eluted at 15.8, 18.8 and 26.9 min. The *N*-glycan profiles were significantly altered in ichthyotic hyperkeratotic skin compared with normal non-hyperkeratotic controls. These findings indicate the reduction of *N*-acetylglucosaminyltransferase II and fucosyltransferase 8 activities. Alteration of *N*-glycan structures in hyperkeratotic skin suggests the biological role of *N*-glycans in keratinization.

Keywords High-performance liquid chromatography · Hyperkeratosis · Neutral oligosaccharide · *N*-Glycan · Oligosaccharide

H. Ito · M. Akiyama (✉) · J. R. McMillan · H. Shimizu
Department of Dermatology,
Hokkaido University Graduate School of Medicine,
North 15 West 7, Sapporo, 060-8638, Japan
e-mail: akiyama@med.hokudai.ac.jp

H. Nakagawa · R. Uematsu · K. Deguchi · S.-I. Nishimura
Division of Biological Sciences,
Frontier Research Center for Post-Genomic
Science and Technology,
Hokkaido University Graduate School of Science,
Sapporo, Japan

R. Uematsu
Research Laboratory, Kanebo Cosmetics Inc.,
Odawara, Japan

J. R. McMillan
Creative Research Initiative Sousei,
Hokkaido University, Sapporo, Japan

Oligosaccharides are known to play important roles in a variety of biological events including cell–cell interactions and undergo modifications during cell differentiation [6]. *N*-Glycan oligosaccharides, which bind to asparagine, are a frequent post-translational modification of proteins. *N*-Glycan oligosaccharides exhibit diversity created by sugar linkages and components including: mannose, galactose, *N*-acetylglucosamine, *N*-acetylneuraminic acid. *N*-Glycan oligosaccharides modify specific protein properties, especially glycoprotein localization, secretion and degradation rates of proteins. Alterations in *N*-glycan composition have been reported in many human diseases [6, 12]. Oligosaccharide analyses using oligosaccharide-specific lectins and antibodies have suggested the biological importance of oligosaccharides in the epidermis [3, 5, 7, 19–21, 25, 28]. However, oligosaccharide-specific lectins and antibodies recognize only two or three sugar residues at most and little information has been obtained from studies with lectins or antibodies concerning the entire range of glycan structures or the *N*-glycan and *O*-glycan composition on glycoproteins and glycolipids. The cellular biosynthesis of *N*-glycan is highly regulated and glycan structures significantly affect protein properties [6, 15]. Alteration of *N*-glycan profiles in diseases have